Image Quality Optimisation and Dose Management in CT, SPECT/CT, and PET/CT

Söderberg, Marcus

2012

Image Quality Optimisation and Dose Management in CT, SPECT/CT, and PET/CT

Marcus Söderberg

Medical Radiation Physics
Department of Clinical Sciences, Malmö
Faculty of Medicine, Lund University
Skåne University Hospital
2012

LUND UNIVERSITY

Thesis for the Degree of Doctor of Philosophy in Medical Science
Lund University
Faculty of Medicine Doctoral Dissertation Series 2012:22
Medical Radiation Physics
Department of Clinical Sciences, Malmö
Skåne University Hospital
SE-205-02 Malmö, Sweden

ISSN 1652-8220
ISBN 978-91-86871-84-0
Printed in Sweden by Media-Tryck, Lund 2012

Executive summary

Medical imaging provides tremendous and undeniable benefits for patients in modern health care. New imaging technologies utilising X-rays and radiopharmaceuticals are continuously being developed. Improvements in the benefit of CT have been so dramatic that a tendency exists to overuse it and not exert enough effort justifying the examination and optimising the technique. Combining two imaging techniques into a single examination, such as SPECT/CT and PET/CT, so-called hybrid imaging, is also increasingly common. The increasing exposure to radiation from CT has been of concern for some years and is now receiving more attention from health professionals, authorities, manufacturers, and patient groups. Another problem is that some of the SPECT and PET investigations contribute a high patient effective dose.

The overall objective of this work was to evaluate and optimise different approaches for minimising patient radiation absorbed dose and maintaining or improving image quality in CT, SPECT/CT, and PET/CT. One way to achieve optimisation is to use automatic exposure control (AEC) systems, which have been shown to be effective at reducing absorbed dose to patients undergoing CT examinations. The dose reduction ranges from 35% to 60% for an anthropomorphic chest phantom, depending on the system and AEC settings. The variation in image noise among images obtained along the scanning direction is lower when using the AEC systems, but the image noise generally increases.

In many X-ray investigations, contrast medium (CM), which is commonly based on iodine, is used to increase detectability. Such intravenous (i.v.) CM can negatively affect kidney function, and the risk of contrast-induced impairment of kidney function increases with age. The lifetime risk for cancer is greater the younger the patient is at the time of exposure. Studies of various patient groups showed that an increased amount of i.v. CM can compensate for a reduced radiation absorbed dose and vice versa, maintaining the signal-to-noise ratio in the liver and contrast-to-noise ratio for a hypothetical hypovascular liver metastasis. Subjective image quality was affected by an increased noise level in the images but was judged to be acceptable in all groups except the one with the lowest radiation absorbed dose. Using this protocol, effective dose was reduced by 57% in the youngest patient group (16-25 years of age) and the amount of i.v. CM was reduced by 18% in the elderly group (>75 years of age).

Organ and effective doses to the patient using a cone-beam O-arm system in spinal surgery were estimated using the Monte Carlo simulation software PCXMC. The highest estimated absorbed doses were in the breast and lungs when scanning the thoracic spine, and stomach when scanning the lumbar spine. The effective dose was reduced to 1.5-2.4 mSv, which is 5 times lower than the scan settings recommended by the manufacturer for intra-operative imaging of the chest and abdominal regions

in a small patient, without a negative impact on image quality in regard to the information required for spinal surgery.

Within the frame of a European project, a new patent-filed phantom, the MADEIRA phantom, has been developed for the investigation of spatial resolution, partial volume effect (intensity diffusion), and detectability in nuclear medicine tomography. The phantom contains a large number of cones that can be filled separately with solutions of different activity concentrations. The phantom has been tested and shows potential as a useful and important practical tool in optimisation work, e.g., for the comparison of reconstruction methods and optimisation of different acquisition and reconstruction parameters in SPECT and PET studies.

New image reconstruction methods are constantly being developed. Based on a rank-order study, three different reconstruction methods were optimised and compared in a visual assessment of ^{123}I-MIBG-SPECT. The patients were examined with a Siemens Symbia T6 SPECT/CT and they were referred for detection of neuroendocrine tumours. The images were presented and evaluated using recently developed viewer software adapted for observer studies with the possibility of showing up to eight unlabeled image sets side-by-side. Of the three reconstruction methods, Siemens Flash 3D using 32 (4 h post-injection) and 16 (24 h post-injection) equivalent iterations were found to be the preferable reconstruction algorithms.

There is still considerable room for optimisation and continuous developments of new technologies aim to optimise image quality and radiation absorbed dose to the patient. Anticipated future developments are photon counting detectors in combination with high atomic number contrast agents, together with comprehensive iterative image reconstruction algorithms, which will allow new medical applications. These developments will continue to require close collaboration between medical physicists, manufacturers, radiologists, nuclear medicine physicians, technologists, and referring physicians in order to be effectively and optimally used. The challenge is to establish sufficient image quality for a specific diagnostic task with the lowest effective dose to the patient.

Summary in Swedish

Det diagnostiska värdet av röntgen- och nuklearmedicinska undersökningar kan knappast överskattas. Däremot innebär undersökningar som baseras på joniserande strålning en liten risk för patienten att senare i livet utveckla en cancer. Därför är det vår skyldighet att hålla stråldoserna så låga som möjligt med bibehållen diagnostisk noggrannhet. Idag utgör medicinska undersökningar en betydande del av befolkningens exponering för joniserande strålning. Dessutom ökar stråldoserna inom sjukvården för varje år och det ökade antalet CT-undersökningar är den största orsaken till denna växande andel av kollektivdosen. Flera av de avbildningstekniker som används idag är ännu inte optimerade med hänsyn till bildkvalitet och patientstråldos. Detta gäller särskilt undersökningar med CT, SPECT/CT och PET/CT. Idag finns det olika metoder för att sänka stråldoserna. Den svåra frågan att utreda är vad som är tillräcklig stråldos för en viss undersökning utan att den diagnostiska säkerheten blir för låg. Det övergripande syftet med denna avhandling är att förbättra och systematiskt utvärdera bildkvalitet och patientstråldos vid bild- och funktionsundersökningar.

Avhandlingen innehåller studier av system för exponeringsautomatik på CT, med vilka rörströmmen anpassas efter varje patients storlek och form samt röntgenstrålningens absorption och spridning. Dessa olika system har utvärderats beträffande sin effektivitet, såväl med avseende på bildkvalitet som patientstråldos. Beroende på system och inställningar minskade absorberad dos med 35-60 % för ett antropomorfiskt thoraxfantom. Brusnivån i bilderna blev mer jämn mellan olika anatomiska regioner även om bruset generellt ökade.

För att förbättra den diagnostiska informationen vid CT-undersökningar tillförs ofta kontrastmedel som kan ha en oönskad påverkan på njurfunktionen, särskilt för äldre patienter. Risken för sena effekter av strålning (cancer) är däremot högst för yngre patienter. Genom att justera mängd kontrastmedel mot stråldos kan risker i olika åldrar minimeras. För yngre patienter (16-25 år) kunde stråldosen mer än halveras. Detta kunde göras genom att mängden kontrastmedel ökades så att signal-till-brus-förhållande i levern bibehölls och kontrast-till-brus-förhållande för en tänkt levermetastas som bara sparsamt fylls med kontrastmedel bibehölls. Hos äldre patienter (>75 år) kunde mängden kontrastmedel minskas med 18 % genom att stråldosen ökades med 46 % för bibehållen bildkvalitet.

Kliniska undersökningsprotokoll för ett mobilt intraoperativt bildsystem (O-arm) bestående av en CT med ett konformat strålknippe har optimerats för användning vid kirurgiska ingrepp i ryggraden. Organdoser och effektiv dos har beräknats genom Monte Carlo simulering och erhållna bilder har bedömts av observatörer. Resultatet visade att effektiv dos kan reduceras till 1,5-2,4 mSv med tillräcklig bildkvalitet för

ändamålet, vilket är 5 gånger lägre stråldos jämfört med de inställningar som tillverkaren angivit för bildtagning av en liten patient.

Inom ramen för ett EU-projekt har ett nytt fantom benämnt MADERIA tagits fram för optimering av nuklearmedicinsk diagnostik. Fantomet är unikt i sin konstruktion med ett stort antal lika stora ihåliga koner vilka kan fyllas med radioaktiva lösningar av olika aktivitetskoncentration. Detta möjliggör studier av rumslig upplösning, partiell volymseffekt (intensitetsdiffusion) och detekterbarhet. Baserat på erfarenhet av olika fantommätningar har fantomet vidareutvecklats. Fantomet har potential att bli ett användbart och viktigt verktyg i optimeringsarbetet av SPECT- och PET-undersökningar.

Ständigt sker det förbättringar och utveckling av nya typer av bildrekonstruktions-metoder. Tre olika rekonstruktionsmetoder för SPECT har optimerats och jämförts i en observatörsstudie av ^{123}I-MIBG-bilder vid misstanke om tumörsjukdom. Bilderna presenterades och rangordnades med hjälp av ett bildvisningsprogram som anpassades för observatörsstudier med möjlighet att visa upp till 8 olika rekonstruktioner sida vid sida. För den nyttjade SPECT-kameran och parameterinställningar bedömdes Siemens algoritm Flash 3D med 32 (4h efter injektion) och 16 (24h efter injektion) ekvivalenta iterationer ge bäst bildkvalitet.

Det finns utrymme för fortsatt optimering av bildkvalitet och stråldos. Ständigt pågår utveckling av ny teknologi som möjliggör detta. Framtida potentiella tekniker såsom energiupplösande detektorer i kombination med kontrastmedel baserade på ämnen med högt atomnummer och förbättrade iterativa bildrekonstruktionsmetoder kommer medföra nya medicinska applikationer. Detta kommer även i fortsättnigen fordra ett nära samarbete mellan sjukhusfysiker, tillverkare, radiologer, nuklearmedicinare, röntgensjuksköterskor, biomedicinska analytiker och remitterande läkare. Målet är att fastställa tillräcklig bildkvalitet för en specifik diagnostisk frågeställning med lägsta möjliga effektiv dos till patienten.

Abbreviations and symbols

AAPM	American Association of Physicists in Medicine
AEC	automatic exposure control
AUC	area under the curve
BEIR	Committee on the Biological Effects of Ionising Radiation, National Research Council (USA)
CBCT	cone-beam computed tomography
CIN	contrast-induced nephropathy
CM	contrast medium
CNR	contrast-to-noise ratio
CT	computed tomography
CTDI	computed tomography dose index
DICOM	digital imaging and communications in medicine
DLP	dose-length product
DECT	dual energy computed tomography
DNA	deoxyribonucleic acid
EI	equivalent iteration
FDG	fluorodeoxyglucose
FBP	filtered back-projection
HU	Hounsfield unit
IAEA	International Atomic Energy Agency
ICRP	International Commission on Radiological Protection
ICRU	International Commission on Radiation Units and Measurements
IEC	International Electrotechnical Commission
i.v.	intravenous
k	DLP to E conversion factor
L	scan length
M	mean value of measured image noise values
MADEIRA	minimising activity and dose with enhanced image quality by radiopharmaceutical administration (European Commission 7th framework programme)
MIBG	metaiodobenzylguanidine
MLEM	maximum likelihood expectation maximisation
MRI	magnetic resonance imaging
MSCT	multi-slice computed tomography
NCRP	National Council on Radiation Protection and Measurements (USA)
OPED	orthogonal polynomial expansion on disc
OSEM	ordered subsets expectation maximisation
PACS	picture archiving and communication system
PET	positron emission tomography
p.i.	post-injection

PVE	partial volume effect (intensity diffusion)
ROC	receiver operating characteristic
ROI	region of interest
SD	standard deviation
SNR	signal-to-noise ratio
SPECT	single photon emission computed tomography
TCM	tube current modulation
VGA	visual grading analysis
VGC	visual grading characteristic
ViewDEX	viewer for digital evaluation of X-ray images
UNSCEAR	United Nations Scientific Committee on the Effects of Atomic Radiation
μ	linear attenuation coefficient
σ	SD of measured image noise values

Original papers

This thesis is based on the following papers, which will be referred to in the text by their Roman numerals. The papers are appended at the end of the thesis.

Ia Söderberg M, Gunnarsson M
Automatic exposure control in computed tomography – an evaluation of systems from different manufacturers
Acta Radiol 2010; 51(6): 625-634

Ib Söderberg M, Gunnarsson M
The effect of different adaptation strengths on image quality and radiation dose using Siemens CARE Dose 4D
Radiat Prot Dosim 2010; 139(1-3): 173-179

II Fält T, Söderberg M, Hörberg L, Carlgren I, Leander P
A seesaw balancing radiation dose and intravenous contrast medium dose – evaluation of a new abdominal CT protocol reducing age-specific risks
Am J Roentgenol (revision requested)

IIIa Söderberg M, Abul-Kasim K, Ohlin A, Gunnarsson M
Estimation of organ and effective dose to the patient during spinal surgery with a cone-beam O-arm system
Proc SPIE 2011; 7961(79613G): 1-6

IIIb Abul-Kasim K, Söderberg M, Selariu E, Gunnarsson M, Kherad M, Ohlin A
Optimization of radiation exposure and image quality of the cone-beam O-arm intraoperative imaging system in spinal surgery
J Spinal Disord Tech 2012; 25(1): 52-58

IV Söderberg M, Engeland U, Mattsson S, Ebel G, Leide-Svegborn S
Initial tests of a new phantom for investigation of spatial resolution, partial volume effect and detectability in nuclear medicine tomography
J Phys Conf Ser 2011; 317(012017): 1-7

V Söderberg M, Mattsson S, Oddstig J, Uusijärvi-Lizana H, Valind S, Thorsson O, Garpered S, Prautzsch T, Tischenko O, Leide-Svegborn S
Evaluation of image reconstruction methods for ^{123}I-MIBG-SPECT: a rank-order study
Acta Radiol (submitted)

Published papers have been reproduced with kind permission of the following publishers:

The Royal Society of Medicine Press Ltd (**Paper Ia**)
Oxford University Press (**Paper Ib**)
Society of Photo Optical Instrumentation Engineers (**Paper IIIa**)
Lippincott Williams & Wilkins (**Paper IIIb**)
IOP Publishing (**Paper IV**)

Preliminary reports

Preliminary reports have been presented at the following conferences:

Söderberg M, Gunnarsson M
The effect of different adaptation strengths on image quality and radiation dose using Siemens CARE Dose 4D
Third Malmö Conference on Medical Imaging, Malmö, Sweden, June 2009

Söderberg M, Gunnarsson M
Automatic exposure control in CT – an evaluation of systems from different manufacturers
The Swedish X-ray Conference (Röntgenveckan), Jönköping, Sweden, September 2009

Söderberg M, Gunnarsson M
Dose reduction and image quality evaluations of automatic exposure control systems from four different CT manufacturers
7th International Conference on Medical Physics in the Baltic States, Kaunas, Lithuania, October 2009

Fält T, Leander P, Söderberg M
A novel concept for contrast-enhanced abdominal CT with age-adjusted radiation and i.v. contrast doses to minimize age-specific risks
European Congress of Radiology, Vienna, Austria, March 2010

Fält T, Söderberg M, Hörberg L, Leander P
A seesaw balancing radiation dose and i.v. contrast medium dose – evaluation of a new abdominal CT protocol reducing age-specific risks
RSNA, Chicago, USA, November 2010

Söderberg M, Abul-Kasim K, Ohlin A, Gunnarsson M
Estimation of organ and effective dose to the patient during spinal surgery with O-arm
SPIE Medical Imaging, Orlando, USA, February 2011

Söderberg M, Engeland U, Mattsson S, Ebel G, Leide-Svegborn S
Initial tests of a new phantom for investigation of spatial resolution, partial volume effect and detectability in nuclear medicine tomography
International Conference in Image Optimisation in Nuclear Medicine, Ayia Napa, Cyprus, March 2011

Abul-Kasim K, Söderberg M, Selariu E, Gunnarsson M, Kherad M, Ohlin A
Optimization of radiation exposure and image quality of the cone-beam O-arm intraoperative imaging system in spinal surgery
18th International Meeting on Advanced Spine Techniques, Copenhagen, Denmark, July 2011

Other related publications by the author

Uusijärvi H, Sydoff M, Söderberg M, Leide-Svegborn S, Mattsson S
Optimising PET/CT and SPECT/CT investigations. The MADEIRA project
Proc 6th International Conference on Medical Physics in the Baltic States 2008: 49-51

Söderberg M, Gunnarsson M, Nilsson M
Simulated dose reduction by adding virtual noise to measured raw data – a validation study
Radiat Prot Dosim 2010; 139(1-3): 71-77

Leander P, Söderberg M, Fält F, Gunnarsson M, Albertsson I
Post-processing image filtration enabling dose-reduction in standard abdominal CT
Radiat Prot Dosim 2010; 139(1-3): 180-185

Mattsson S, Söderberg M
Patient dose management in CT, PET/CT and SPECT/CT imaging
Proc 8th International Conference on Medical Physics in the Baltic States 2010: 18-23

Mattsson S, Söderberg M
Radiation dose management in CT, SPECT/CT and PET/CT techniques
Radiat Prot Dosim 2011; 147(1-2): 13-21

Giussani A, Janzen T, Uusijärvi-Lizana H, Tavola F, Zankl M, Sydoff M, Bjartell A, Leide-Svegborn S, Söderberg M, Mattsson S, Hoeschen C, Cantone M.C
A compartmental model for biokinetics and dosimetry of ^{18}F-choline in prostate cancer patients
Accepted for publication in J Nucl Med 2012

Contents

1. Introduction

Medical imaging provides tremendous and undeniable benefits for patients in modern health care. Imaging is used for a broad range of tasks, including disease detection, classification, prognostic staging, treatment planning, and validation of therapeutic responses. During recent years, substantial developments have been made in imaging techniques with progress continuing today. Computed tomography (CT) (Hounsfield, 1976) and magnetic resonance imaging (MRI) (Damadian, 1971) have become important imaging techniques since their introduction in clinical practise in the 1970s and 1980s, respectively. They have supplemented, and in some cases even replaced, planar X-ray, nuclear medicine, and ultrasound (Mattsson et al., 2010).

After the introduction of multi-slice CT (MSCT) in 1997 (Hu, 1999), the number of slices acquired per rotation has rapidly increased from 4 up to 8, 16, 32, 40, 64, 128, and 320 (Hsieh, 2009). The primary advantage of MSCT is improved temporal (<250 ms) and spatial resolution (<0.5 mm) and shorter scan times (Flohr and Ohnesorge, 2007). However, shortcomings and pitfalls with increased detector width have revealed more scattered radiation, introduced cone-beam artefacts, and helical over-scanning. Today, beam widths are up to 160 mm, making the current paradigm for characterising radiation absorbed dose in CT by means of the computed tomography dose index (CTDI) no longer appropriate (American Association of Physicists in Medicine: AAPM, 2010).

The objectives in CT development have changed from increasing the number of slices to focusing on improvements in X-ray tube performance, detector efficiency, and data processing (Fleischmann and Boas, 2011). Since 2006, a new scanner technology using two X-ray sources and two detectors simultaneously, dual source CT, has been available (Johnson and Kalender, 2011). The technology has provided further improvements in scan speed and temporal resolution (0.28 s rotation time and 75 ms temporal resolution). By utilizing dual energy CT (DECT), using either dual source or kV-switching, and advanced post-processing and visualisation, new clinical applications have been found. The advantage with DECT is that the properties of X-ray attenuation change at different energies, which are used to differentiate materials, including iodine, calcium, and uric acid crystals. In recent years, iterative reconstruction methods have been introduced that provide great potential for improving image quality and reduced radiation doses (Hsieh, 2009).

Large-area flat panel detectors in combination with cone beam X-ray fields (cone-beam CT, CBCT) are now used more frequently as an alternative to conventional CT (Gupta et al., 2008). Examples of CBCT applications include interventional and intra-operative imaging, image-guided external tumour therapy, maxillofacial scanning, and breast imaging. Moreover, flat panel detector technology is also applied

to standard CT. As mentioned above, the coverage of a large volume per rotation has led to demands for a new framework for characterising the absorbed dose.

In addition to CT development, diagnostic imaging has evolved from standalone techniques to combined (hybrid) imaging (Beekman and Hutton, 2007; Townsend, 2008). The nuclear medicine methods single photon emission computed tomography (SPECT) (Kuhl and Edwards, 1963) and positron emission tomography (PET) (Brownell et al., 1971) have been shown to improve diagnostic accuracy in a variety of clinical applications when used in combination with CT (Hicks et al., 2007; Townsend, 2008). The complementary anatomical, functional, and molecular information provided by these hybrid techniques has proven clinical importance, e.g., the molecular process of a tumour can be accurately identified and localised to a specific tissue or organ. There is also potential for improving SPECT and PET image reconstruction and quantification, e.g., using the CT data for attenuation correction. PET/MR systems are also currently being evaluated clinically (Ratib and Beyer, 2011). One of the advantages of MRI is greater soft tissue contrast and an ability to change the contrast. The primary advantage of SPECT and PET compared to other medical imaging modalities is high sensitivity with a superior capacity to localise low concentrations of a radiotracer at the target (Eckelman et al., 2008). The disadvantage with these two imaging techniques is the limited spatial resolution (SPECT: 4-12 mm, PET: 4-6 mm).

The improvements in CT technology have led to an increased use of CT, and it has replaced several radiographic examinations. A report from the Swedish Radiation Safety Authority (Almén et al., 2008) showed that the number of CT investigations in Sweden increased by 100% between 1995 and 2005. The report also showed that CT and nuclear medicine constituted 16% of all radiological investigations (excluding mammography and dental examinations) and contributed to 64% of the collective effective dose in Sweden in 2005 (Figure 1.1). The National Council on Radiation Protection and Measurements (NCRP, 2009) in the USA reported that CT and nuclear medicine constituted 22% of all radiological investigations but 75% of the collective US radiation effective dose in 2006.

The significant increase in the use of CT, alone or combined with SPECT or PET, has raised concerns about patient radiation exposure and the consequent increased risk of malignancy later in life (Brenner and Hall, 2007; International Commission on Radiological Protection: ICRP, 2000; 2007b; United Nations Scientific Committee on the Effects of Atomic Radiation: UNSCEAR, 2008). Another problem is that some of the PET and SPECT investigations give a high patient effective dose compared to the majority of planar X-ray investigations.

The introduction of PET and PET/CT techniques and increasing use of positron emitters have also increased radiation doses to staff at hospitals, including the staff at the cyclotrons and hot laboratories used for the production of radiopharmaceuticals (Mattsson and Söderberg, 2011a).

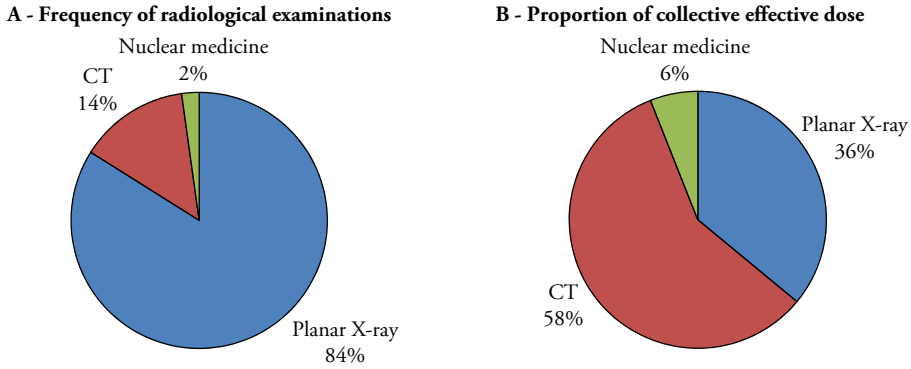

Figure 1.1 Although CT and nuclear medicine examinations contribute a relatively low percentage of the total number of diagnostic radiological examinations (excluding mammography and dental examinations) (A), CT and nuclear medicine contribute a high proportion of the collective effective dose (B). The figure refers to data from Sweden in 2005 (Almén et al., 2008).

The gradually increasing awareness of radiation exposure mainly from CT examinations has forced manufacturers to develop techniques to reduce radiation doses. The implementation of these methods, as well as recommendations from authorities, requires close collaboration between medical physicists, manufacturers, radiologists, nuclear medicine physicians, technologists, and referring physicians in order to be effective. The challenge is to establish sufficient image quality for a specific diagnostic task with the lowest effective dose to the patient.

1.1 Objectives

The overall objective of this work was to evaluate and optimise different approaches for minimising patient radiation absorbed dose and maintaining or improving image quality in CT, SPECT/CT, and PET/CT. The specific objectives were:

- To evaluate AEC systems from different CT scanner manufacturers in terms of their potential for reducing absorbed dose to the patient while maintaining adequate image quality (**Papers Ia** and **Ib**).
- To evaluate an abdominal CT protocol reducing age-specific risks by balancing absorbed dose and the amount of intravenous (i.v.) contrast medium (CM) (**Paper II**).
- To estimate and optimise the absorbed dose and image quality of a new cone-beam O-arm imaging system for use in spinal surgery (**Papers IIIa** and **IIIb**).
- To describe and perform initial tests of a new phantom aimed at investigating spatial resolution, partial volume effect (PVE), and detectability in nuclear medicine tomography (**Paper IV**).
- To evaluate the influence of different image reconstruction methods on ^{123}I-metaiodobenzyl-guanidine (MIBG)-SPECT images using a rank-order study (**Paper V**).

2. Background

2.1 Dosimetry

CT scanners generate cross-sectional images by measuring X-ray attenuation properties from multiple directions around the region of interest when the X-ray tube and detector are rotated around the object (Kalender, 2005). When the X-rays penetrate the object, parts of its energy is absorbed by the object. The amount of energy imparted per unit mass at a point is expressed in terms of absorbed dose as defined by the International Commission on Radiation Units and Measurement (ICRU, 1998). The absorbed dose is the fundamental dosimetric quantity, and its unit is joule per kilogram, denoted as gray (Gy). To assess radiation exposure to humans and correlate it with the risk of exposure, mean absorbed dose in an organ or tissue is used (ICRP, 2007b). Based on the dose quantities prescribed by the ICRU and ICRP, the International Atomic Energy Agency (IAEA) has established an international code of practice for dosimetry in diagnostic radiology (IAEA, 2007).

SPECT (Zeng et al. 2004) and PET (Lewellen and Karp, 2004) are imaging techniques using radiopharmaceuticals. The tracer compounds are labelled with single photon or positron-emitting radionuclides, respectively, and injected into the subject prior to the investigation. The radionuclide in the radiotracer decays, and the resulting photons are detected by surrounding external detectors. Parts of the emitted energy from the decays will be absorbed by the body, which is expressed in terms of mean absorbed dose. The signal acquired by the detectors is used to reconstruct the radiopharmaceutical distribution throughout the patient.

2.1.1 The principles of CT dosimetry

For CT, estimates of absorbed doses to organs and tissues and effective doses are based on two quantities: CTDI and dose-length product (DLP) (AAPM, 2008). The CTDI concept was originally introduced for single slice axial scanning (Shope et al., 1981). CTDI represents the average absorbed dose along the z-axis (table feed direction) from a series of contiguous irradiations. The most commonly used index is $CTDI_{100}$, which refers to absorbed dose in air or in cylindrical polymethyl methacrylate phantoms (15 cm in length) representing head (16 cm in diameter) and body (32 cm in diameter). The International Electrotechnical Commission (IEC, 2009) has defined $CTDI_{100}$ as the absorbed dose integrated over a length of 100 mm for a single axial scan using a pencil ionisation chamber with an active length of 100 mm, divided by the collimated beam width (if $n \cdot T < 100$ mm) or 100 mm (if $n \cdot T \geq 100$ mm):

$$CTDI_{100} = \int_{-50mm}^{+50mm} \frac{D(z)}{\min\{n \cdot T,\ 100\ mm\}} dz \tag{2.1}$$

where n is the number of slices per rotation, T is the nominal slice thickness, and D(z) is the absorbed dose profile along the z-axis. To account for spatial variation of the absorbed dose in the scan plane (x, y), a weighted dose index ($CTDI_w$) was introduced (Leitz et al., 1995):

$$CTDI_w = \frac{1}{3} CTDI_{100(central)} + \frac{2}{3} CTDI_{100(peripheral)} \tag{2.2}$$

To take axial scan spacing into account, CTDI by volume ($CTDI_{vol}$) was introduced (Bongartz et al., 2004):

$$CTDI_{vol} = \frac{CTDI_w}{pitch} \tag{2.3}$$

where pitch is defined as the ratio of the table transportation per rotation to the collimated beam width (Silverman, 2001). $CTDI_{vol}$ is expressed in mGy and is displayed on the CT consoles. The $CTDI_{vol}$ is a measure of the radiation output of a CT scanner and represents an estimation of the average absorbed dose within the irradiated volume of an object of similar attenuation to the CTDI phantom. $CTDI_{vol}$ needs to be adjusted for patient size because it does not represent the average absorbed dose for objects of substantially different size or shape (AAPM, 2011).

To better represent the overall energy delivered for an entire CT exam, DLP expressed in mGy·cm was introduced (Bongartz et al., 2004):

$$DLP = CTDI_{vol} \cdot L \tag{2.4}$$

where L is the scan length. DLP is a measure of the total energy deposited in the phantom or patient.

The quantity effective dose is the sum of weighted equivalent doses in the principal tissues and organs of the body (ICRP, 1991; 2007b). The different tissues and organs have been assigned a tissue weighting factor that reflect the radiosensitivity. The equivalent dose expresses the biological impact of a given type of radiation. Consequently, effective dose reflects the stochastic risk, such as cancer induction, and the unit is sievert (Sv) (ICRP, 1991). Broad estimates of the effective dose can be obtained by multiplying DLP by a conversion factor (k) appropriate to different anatomical regions (Bongatz et al., 2004; Huda et al., 2008; Shrimpton, 2004):

$$E = DLP \cdot k \tag{2.5}$$

The conversion factors (Table 2.1) are averaged over all photon energy distributions used in different scanners, and obtained from Monte Carlo simulation and mathematically describable phantoms representing adult and paediatric patients. The factors are useful for quick dose estimates and for large patient groups. Conversion factors for DLP to effective dose for different tube voltages, regions, and ages based on the latest tissue-weighting factors from ICRP (2007b) were recently determined by Deak et al. (2010) and are valid for a Siemens Sensation 64 CT scanner (Table 2.1). The tissue weighting factors were modified by ICRP due to new available scientific data. For a more detailed assessment of effective dose and organ absorbed doses, dose assessment software, such as CT-Expo (Stamm and Nagel, 2002) and ImPACT CT patient dosimetry calculator (Keat, 2011), are recommended.

The effective dose from a CT investigation typically ranges from 2 mSv (head) to 10 mSv (abdomen and pelvis), but with large variations between patients and hospitals. A total body investigation (brain, chest, abdomen, and pelvis) provides about 20 mSv (ICRP, 2007a). This is roughly a factor of 10 to 100 higher than typical conventional planar X-ray investigations (range of 0.01-10 mSv). For example, the effective dose for a hand radiograph is less than 0.1 mSv. CT doses are highly dependent on the characteristics of the CT scanner, patient size, anatomical region under investigation, and scanning parameters used in each examination. For some individuals, local organ and tissue doses from a CT investigation can be up to 100 mSv (ICRP, 2007a; UNSCEAR, 2010).

Table 2.1 Conversion factor k (mSv mGy^{-1} cm^{-1}) for DLP to effective dose for various body regions in adults and paediatric patients of various ages. Conversion factors based on tissue-weighting factors from ICRP Publication 60 (1991) valid for single-slice CT scanners have been published by Bongartz et al. (2004), and conversion factors based on tissue-weighting factors from ICRP Publication 103 (2007b) valid for a 64-slice CT scanner have been published by Deak et al. (2010).

	ICRP 60	**ICRP 103**				
Region of body	**Adult**	**Adult**	**10 years**	**5 years**	**1 year**	**Newborn**
Head	0.0023	0.0019	0.0027	0.0035	0.0054	0.0087
Neck	0.0054	0.0052	0.0094	0.0121	0.0168	0.021
Chest	0.019	0.0146	0.0237	0.0323	0.0482	0.0739
Abdomen	0.017	0.0153	0.0249	0.0357	0.053	0.0841
Pelvis	0.017	0.0129	0.0219	0.03	0.0446	0.0701
Legs	0.0008	-	-	-	-	-

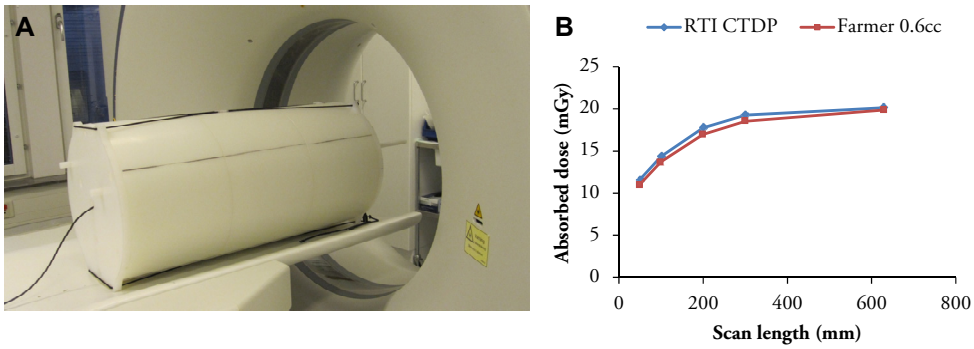

Figure 2.1 The new phantom designed by AAPM and ICRU consists of three sections, making it possible, in the future, to evaluate noise power spectrum and modulation transfer function (A). The equilibrium dose as a function of scan length measured centrally in the phantom with two different detectors (B).

The CTDI methodology, which is based on the assumption that the beam width in the z-axis is substantially smaller than 100 mm, currently has some limitations (Boone, 2007). As the radiation beam widths of MSCT scanners get wider and various CBCT systems are introduced, this method of estimation becomes more inappropriate. When the primary beam is nearly the same size or larger than the length of the probe, the dose will be underestimated because a portion of leakage and scattered radiation will not be measured. A new measurement paradigm was recently proposed (AAPM, 2010; Dixon and Boone, 2010). Implementation of these recommendations is currently being evaluated by the AAPM task group 200 and ICRU. A new polyethylene-based phantom has been designed, measuring 30 cm in diameter and 60 cm in length, to quantify the equilibrium dose (Figure 2.1). The equilibrium dose can be measured by a small radiation detector in the phantom that is long enough to capture the entire scatter tails.

2.1.2 The principles of dosimetry in nuclear medicine

In nuclear medicine investigations, the administered activity is the basic measurable quantity. The absorbed dose to a patient undergoing a SPECT or PET investigation is based on the physical properties of the radionuclide and biological behaviour of the administered radiopharmaceutical. Using standardised biokinetic and dosimetric models (ICRP, 1988; 2008; Stabin, 2006), organ/tissue doses and effective doses per unit of administered activity are given by the ICRP (1988; 1998; 2008). Using mathematical/computational phantoms described by Cristy and Eckerman (1987), dose calculations were performed for adults and children (15, 10, 5, or 1 year old).

Updated information concerning the mean absorbed doses to organs and tissues of patients of various ages is available for over 190 radiopharmaceuticals in common use. A number of generic models and realistic maximum models are also available for other large substance groups (ICRP, 2008). Today, voxel-based phantoms based on CT or MRI examinations of human beings are available for adults (Hadid et al., 2010; ICRP, 2009). These phantoms will replace the mathematical phantoms in dosimetric models used by ICRP when voxel-based phantoms representing children are available. The voxel-based phantoms provide more realistic information about human anatomy and permit more detailed dose calculations.

The radiation absorbed dose to a patient depends on the injected activity, radionuclide, tracer, patient biology, and patient geometry. Effective doses from PET and SPECT investigations are considerable compared to conventional X-ray examinations. A common PET investigation with ^{18}F-fluorodeoxyglucose (FDG) provides 7.6 mSv from 400 MBq (0.019 mSv MBq^{-1}) in an adult (ICRP, 2008). For the majority of ^{99m}Tc substances used for SPECT, the effective dose per unit activity is very similar from substance to substance (0.005-0.02 mSv MBq^{-1}) (Mattsson et al., 2011b). A typical bone SPECT investigation using 600 MBq ^{99m}Tc-phosphate provides 3.4 mSv to an adult (ICRP, 2008). PET/CT and SPECT/CT have replaced standalone PET and SPECT in many applications. Consequently, two high-dose investigations are combined, leading to effective doses up to 25 mSv. However, this can be reduced to about 10 mSv when a low-dose CT is used for attenuation correction and anatomical localisation only.

2.1.3 Radiation risks related to medical imaging

Ionising radiation, such as X-rays and gamma radiation, may interact in the human body and indirectly or directly cause damage to the deoxyribonucleic acid (DNA) of the various tissue cells, which may induce late or acute effects. Evidence indicates that exposure to high doses of ionising radiation (>100 mSv) is a risk factor for cancer development, i.e. stochastic effects (Brenner et al., 2003; UNSCEAR, 2008). However, there is still debate concerning the risks imposed by lower doses of exposure associated with radiological examinations, such as CT, SPECT, and PET (UNSCEAR, 2011). The general consensus is that a linear relationship exists between radiation dose and cancer risk, even at low radiation doses (ICRP, 1991; 2007b). This linear no-threshold theory is based primarily on large epidemiological studies demonstrating increased cancer incidence among Japanese atomic bomb survivors (Preston et al., 2003). According to ICRP, the risk of developing a lethal cancer is approximately 5% per sievert. The lifetime risk for cancer has been shown to be greater the younger the patient is at the time of exposure because paediatric tissues are more radiosensitive and the expected life time with the risk of developing a radiation-induced effect is longer (Brenner and Hall, 2007). Deterministic effects, such as skin injuries, cataracts, and hair loss, must also be considered. Recently, the media in the

United States have reported on accidental radiation overdoses in which patients underwent CT brain perfusion and experienced temporary hair loss (3-5 Gy).

However, medical imaging usually provides an accurate and important diagnosis, thereby saving many lives. The most reasonable policy is to maintain a cautious approach to the medical use of ionising radiation, most importantly in younger patients. An examination should be performed only when it is justified to avoid unnecessary irradiation of the patients. Other diagnostic methods utilising non-ionising radiation, such as ultrasound and MRI, should be considered when possible, taking into account economic and societal factors. The justification of an investigation and the role of the involved staff are clarified in ICRP Publication 103 (2007b). The concept justification involves many factors, such as adequate referral, optimised patient exposure, and correct diagnosis corresponding to the request. The benefit for the patient should always be greater than the expected harm.

The Swedish Radiation Safety Authority (Almén et al., 2009) has evaluated referrals for all CT examinations conducted in Sweden during one day in 2006. They found that approximately 20% of all CT examinations were not justified, but this strongly depended on the examined organ. A study by Oikarinen et al. (2009) reported that approximately 30% of 200 CT examinations on patients under 35 years of age were unjustified. The researchers decided as to whether an examination was justified based on recommended referral criteria from the European Commission (2001). The majority of the unjustified examinations could have been replaced by MRI. Consequently, if unjustified examinations are reduced, a major dose reduction would be achieved.

According to the ICRP (2007b), the quantity effective dose can have practical value for comparing the relative doses related to the stochastic effects of internal and external exposures from various diagnostic examinations in different hospitals. Effective dose is also useful for comparing different technologies for the same medical examination, provided that the representative patients or patient populations for which the effective doses are derived are similar with regard to age and gender. Effective dose does not relate to individuals, but to reference persons. However, comparisons of effective doses are inappropriate for risk assessments when significant dissimilarities exist between the age and gender distributions of the representative patients or patient populations being compared (e.g., children, all females, and elderly populations). This is a consequence of the magnitudes of risk for stochastic effects being dependent on age and gender. Risk assessments for medical uses of ionising radiation are best evaluated using appropriate risk values for the individual tissues at risk, and for the age and gender distribution of the population groups undergoing the procedures. The Committee on the Biological Effects of Ionising Radiation (BEIR, 2006) has derived risk models for both cancer incidence and cancer mortality.

2.1.4 Methodologies for dose reduction

Recent technological advances have increased the number of clinical applications for CT. Due to the increased number of examinations CT is the largest source of medical radiation exposure to the general population (Almén et al., 2008). The reduction in CT doses during recent years has been significant, mainly due to improved technology from manufacturers and increasing awareness at the operator level of the importance of acquisition parameters for patient dose (ICRP, 2007a). Technological advancements have resulted in an increased scan speed, a capacity to provide large scan coverage, better contrast utilisation, less image noise, increased spatial resolution, and improved temporal resolution. For example, today a cardiac CT scan can be performed at an effective dose of roughly 1 mSv using electrocardiogram-based tube current modulation (TCM). A decade ago the effective dose for a cardiac examination was up to 20 mSv, depending on scanner-specific factors and acquisition protocol (Mayo and Leipsic, 2009).

Several methods are available to optimise and minimise the radiation absorbed doses in CT (Kalender et al., 2008; Kalra et al., 2004; Mattsson and Söderberg, 2011a). The *scanning parameters* should be optimised for each specific examination and special efforts should be made with paediatric CT protocols (Frush, 2008). A number of scanning parameters influence patient radiation dose and image quality: tube current, tube voltage, filtration, collimation, reconstruction method, reconstruction filter, slice thickness, pitch, and scanning length (Kalra et al., 2004). The operator can monitor most of these parameters and modify them to obtain the necessary image quality with a minimal absorbed dose to the patient. A simple relationship exists between the tube load (the product of tube current and exposure time per rotation, mAs) and radiation dose to the patient. A 50% reduction in tube load reduces the radiation dose by half (and reduces the detector signal), but also increases the noise level by a factor of $\sqrt{2}$. An adequate mAs level can be determined using dose reduction simulation software (Söderberg et al., 2010). The software adds artificial noise to the CT raw data to simulate a scan acquired with lower dose (mAs). The tube voltage determines the energy of the emitted photons from the X-ray tube; consequently, a variation in tube voltage changes the radiation dose and image quality. Reduction in tube voltage results in reduced radiation dose when all other parameters are held constant. This will increase the image noise and cause contrast changes. Several studies have demonstrated an ability to affect radiation dose and image quality by using a lower tube voltage (Funama et al., 2005; Kalender et al., 2009). A current commercial technology called CARE kV from Siemens Medical Solutions (Forchheim, Germany) automatically adapts the tube voltage and tube current for each patient and clinical indication. The aim is to optimise the contrast-to-noise ratio (CNR) and minimise the absorbed dose.

Protection of radiosensitive organs, such as the breast, eye lens, and gonads, is especially important in paediatric patients, adolescents, and young adults. However, the use of

protective shields made of bismuth or other materials with a high atomic number over sensitive organs during CT investigations is controversial. The shields may cause streak and beam hardening artefacts, increase noise, and result in inaccurate CT numbers (Vollmar and Kalender, 2008). Organ-based TCM in which the tube current is reduced for a certain range of rotation was developed recently to protect radiosensitive organs from direct exposure. Wang et al. (2011a) concluded that the use of organ-based TCM resulted in a similar reduction in the dose to the breast as achieved with bismuth shielding without affecting image noise or CT number accuracy.

The phenomenon of *over-scanning* is the exposure of tissue that is not reconstructed in tomographic images (Hsieh, 2009). Due to reconstruction requirements, helical CT scans start and end beyond the region of reconstruction. As the X-ray beams in modern CT scanners become broader, more and more wasted radiation is delivered to the patient by over-scanning (Tzedakis et al., 2005). One solution to this issue is the use of dynamic collimator technique. Christner et al. (2010) showed considerable dose reductions dependent on scanning length and examination using dynamically adjustable z-axis collimation.

In conjunction with the use of lower doses, several attempts have been made to *filter images* to achieve noise reduction. Leander et al. (2010) showed significant improvement when using adaptive non-linear post-processing in adult abdominal CT. Similarly, Ledenius et al. (2010) found dose reductions of more than 10% for CT brain examinations in patients aged 6-10 years using an image-enhancing filter. However, post-processing image filtration has had reduced importance since the introduction of iterative reconstruction.

Iterative image reconstruction methods have played a role in SPECT and PET for many years (section 2.2.1), but they were only recently made available for CT, thanks to improved computer capacity (Nelson et al., 2011). The conventional filtered back-projection (FBP) procedure is now being replaced. The iterative algorithms have the ability to incorporate statistical models and models of the CT system into the reconstruction process. The potential advantages include decreased image noise, improved spatial resolution, and reduced image artefacts (beam hardening, 'windmill' and metal artefacts), allowing for reduced radiation dose. Different CT manufacturers use different methods to reconstruct the images (Nelson et al., 2011). The iterative process can be performed on image data, projection data (raw data), or a combination of both. Thus far, a couple of clinical studies have shown that iterative reconstruction allows large dose reductions while maintaining image quality compared to FBP (Korn et al., 2011; Prakash et al., 2010; Winklehner et al., 2011). Similar studies can be expected in the near future as the iterative algorithms become more widespread.

Dose reduction can be achieved in SPECT and PET by using tracers with shorter physical and biological half-lives; scaling injected activity by patient weight, body mass index, or body area; or using high-sensitivity PET scanners or high-sensitivity

SPECT collimators (Mattsson and Söderberg, 2011a). As technology and staff awareness increases, the recommended activities of different radiopharmaceuticals may decrease. The radiation dose may also be reduced by combining new iterative reconstruction methods and dedicated collimators and detectors.

Using SPECT/CT and PET/CT, there are two alternatives for CT investigation: a 'low-dose CT' used only for attenuation correction of the SPECT or PET image and anatomical localisation, or an ordinary 'diagnostic CT'. From the point of view of radiation protection, it is essential that diagnostic CT, if needed, be taken as part of the SPECT/CT or PET/CT investigation in order to avoid an unnecessary additional CT examination.

Automatic exposure control in CT

In CT, automatic exposure control (AEC) automatically modulates the tube current in the x-y plane (angular modulation), along the scanning direction (z-axis; longitudinal modulation), or both (combined modulation) (Kalra et al., 2005) (Figure 2.2). The modulation is performed according to the patient's size, shape, and the attenuation of the body parts being scanned. The system adjusts the tube current to obtain the pre-determined image quality indicated by the operator (Table 2.2) with improved radiation efficiency. The adaptation of the tube current is based on attenuation data from the localisation radiograph and attenuation profiles or feedback from online measurements. AEC systems have a number of benefits: better control of the absorbed dose to the patient, improved consistency of image quality among patients, reduction of certain image artefacts, and reduced load on the X-ray tube, which increases its lifetime (Keat, 2005).

Table 2.2 The AEC systems for CT from each manufacturer and methods for setting the level of required image quality (indicator marked in italics) (McCollough et al., 2006).

Manufacturer	AEC system	Method for setting required image quality
GE	AutomA 3D	Specify a *noise index* (approximately equal to SD in a homogenous phantom), min and max mA limits.
Philips	DoseRight	*Protocol mAs* is set for a previously saved reference patient. Tube current is adapted to achieve the same noise level.
Siemens	CARE Dose 4D	*Quality reference mAs* is set for a standard patient. Tube current is adapted relative to the reference value.
Toshiba	SureExposure 3D	Specify a *SD* (equal to SD in a homogenous phantom), min and max mA limits.

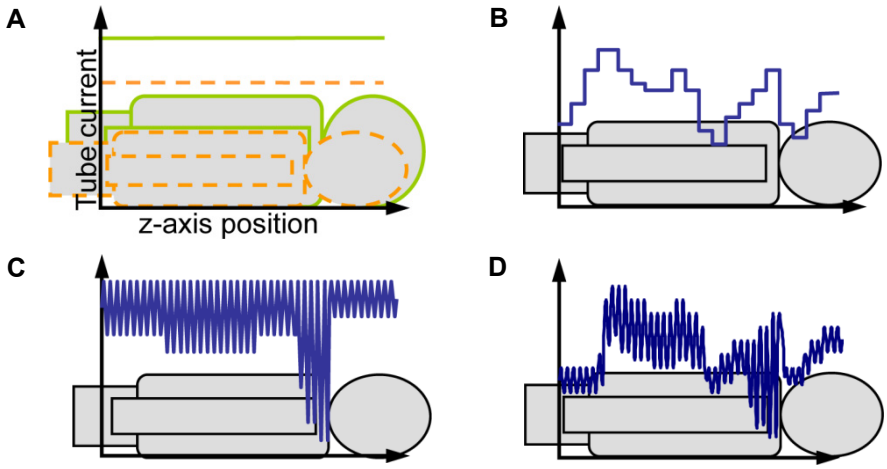

Figure 2.2 Illustrations of different AEC techniques in CT. Patient size AEC, lower tube current (mA) is used for a smaller patient (A), longitudinal AEC, lower mA is used for lower attenuating regions along the z-axis (B), angular AEC, based on asymmetry the mA is adjusted during the course of each rotation (C), combined AEC, a combination of the three techniques (D). Reproduced from Keat (2005) with permission from RSM Press.

All modern CT systems are delivered with AEC systems that modulate tube current in three dimensions. Each of these systems has different specifications and operates somewhat differently. However, the main principle is to manage the required image quality and radiation dose in a reproducible manner by adapting the tube current to the patient's size, shape, and attenuation.

2.1.5 Amount of intravenous contrast medium and related risks

Often, a need for contrast-enhanced CT examination exists in order to achieve a higher contrast between two different nearby structures. By using a contrast medium (CM), which is commonly iodine based and administered intravenously or orally, the arteries, veins, tissues, and organs it courses through will be better visualised due to greater absorption and scattering of the X-rays. Several factors affect the contrast enhancement, which may be divided into three categories: patient (e.g., target organ, weight, cardiac output), contrast medium (e.g., amount of CM, injection duration), and CT scanning (e.g., scan duration, scan delay, radiation) (Bae, 2010). In addition, the radiation dose may be reduced if the CM achieves higher contrast between normal and diseased tissue (Watanbe et al., 2010).

However, such intravenous (i.v.) X-ray CM can negatively affect kidney function and induce nephropathy (CIN) (Stacul et al., 2011). CIN is defined as an increase in creatinine of more than 25% or 44 μmol l^{-1} within 3 days of the administration of

CM (Morcos et al., 1999). CIN is associated with prolonged hospitalisation, dialysis, increased morbidity and mortality (Solomon et al., 2009). The risk of CIN is related to the amount of CM and the number of risk factors. Important risk factors are reduced renal function, congestive heart failure, diabetes, and age over 70 years (Morcos et al., 1999; Stacul et al., 2011). CIN is uncommon in patients with normal renal function (Katzberg and Newhouse, 2010). According to different studies, the incidence of CIN varies widely among patients at increased risk due to lack of uniformity in the definition of CIN, presence or absence of risk factors, amount and type of CM, and type of radiologic procedure (Katzberg and Barrett, 2007; Rundback et al., 2011; Toprak and Cirit, 2006). In patients with multiple risk factors, the risk of CIN can rise to ~50% and the incidence of CIN requiring dialysis in patients has been reported to reach ~15% (McCullough et al., 2006). Recent reports indicate that the risk for CIN may be overstated (Bruce et al., 2009; Katzberg and Newhouse, 2010). However, keeping the amount of i.v. CM administered to patients with risk factors and the elderly to a minimum is still important. Sterner et al. (2009) pointed out that better understanding of risk markers and follow-up of patients exposed to CM are needed. Non-kidney adverse reactions may also occur after contrast injection, e.g. nausea, vomiting, itching and skin rash. However, the use of modern low-osmolality non-ionic CM, these adverse reactions are rare, unpredictable, and independent of the amount of CM (Namasivayam et al., 2006).

2.2 Image quality

In a CT system, the linear attenuation coefficient (μ) is determined, which describes how the X-ray fluence rate is reduced by the object. The attenuation coefficient is presented as CT number relative to the attenuation of water. CT numbers (the signal) are given in Hounsfield units (HU) and, for an arbitrary tissue with attenuation coefficient μ_{tissue}, is defined as (Kalender, 2005):

$$CT\ number = \frac{\mu_{tissue} - \mu_{water}}{\mu_{water}} \cdot 100\ HU \tag{2.6}$$

Ideally, all pixel values would be zero when inserting a region of interest (ROI) in a homogenous water phantom. In reality, the values will be distributed around a mean value and the standard deviation (SD) is often used as a quantified measure of noise. Image noise has two main contributions in CT: quantum noise characterised by Poisson distribution and electronic noise that arises from the data acquisition system. However, SD is not a complete description of image noise as it provides no information about the noise spatial characteristics, i.e. the noise can have different textures. A noise power spectrum reflects the degree of randomness at each spatial frequency and the shape reveals where the noise power is concentrated in frequency

space (Dobbins, 2000). The signal-to-noise ratio (SNR) is a description of the relationship between attenuation and image noise in a specified area. The difference in attenuation between adjacent structures, i.e. the contrast, has greater implications for the diagnostic use of images. The lower the contrast between two structures, the more their conspicuousness is reduced by the increased noise. This relationship is described by the contrast-to-noise ratio (CNR).

In nuclear medicine the signal is characterised by the number of counts; fewer counts result in a higher noise level in the image. The CNR of lesion to background is essential for the detection of lesions in SPECT and PET images. Spatial resolution refers to the ability of the system to depict variations in the distribution of radioactivity in the object. Because a limited spatial resolution volume is defined by the camera, collimator, radionuclide, acquisition protocol, and reconstruction method, the size of the lesion is also important. Below a certain volume, the reconstructed intensity tends to diffuse into neighbouring voxels 'spill-out', resulting in low target-to-background ratios (under-estimation of activity concentration in the target) (Hoffman et al., 1979). This effect is called the partial volume effect (PVE) or, as proposed by Skretting (2009), intensity diffusion (Figure 2.3). PVE may also involve another effect if the target is surrounded by background activity; the target signal will have a contamination component from the surrounding 'spill-in' (over-estimation of the concentration of activity in the target) (Rousset and Zaidi, 2006).

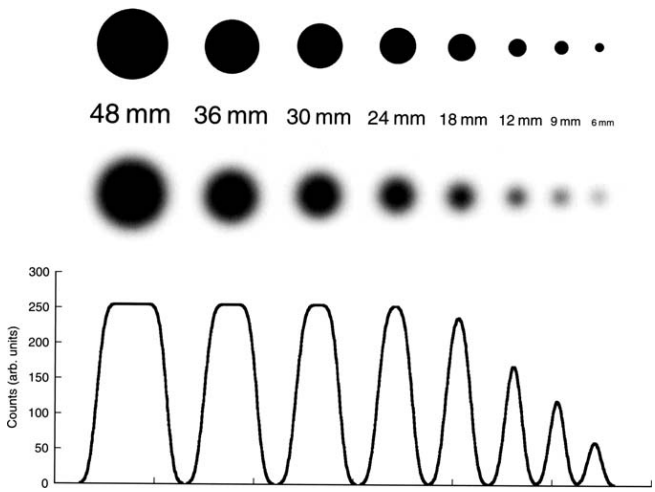

Figure 2.3 Illustration of PVE. The upper row shows cylinders of different diameters containing the same concentration of radionuclide. The middle row shows simulated SPECT images of the cylinders with an in-plane spatial resolution of 12 mm, full width at half maximum. One assumption is that the height of the cylinders is much greater than the axial resolution. The bottom row shows a profile through the centre of the images. Due to the PVE, the intensity decreases when the cylinder size approaches the resolution of the SPECT system. Reproduced from Cherry et al. (2003) with permission from Elsevier.

Several methods can be used to evaluate an imaging system (ICRU, 1996). Physical measures, such as detective quantum efficiency, take both the detector sensitivity and resolution properties into account and describe how an imaging system maintains the SNR (Båth, 2010). However, to predict the diagnostic potential and evaluate what sufficient image quality is for diagnosis in a specific examination, subjective evaluation is essential. Several types of observer performance studies have been used (Månsson, 2000). The choice of human observer study is dependent on the type of examination and conditions. Receiver operating characteristic (ROC) studies are appropriate when a specific diagnostic task is investigated, i.e. when the task for the observer is to state pathological or normal findings (ICRU, 2008). Another approach is visual grading analysis (VGA), in which the reproduction or visibility of certain anatomical structures is assessed. VGA can be performed absolutely or relatively using one or several images as references. An underlying assumption is that pathological findings correlate with the reproduction of normal anatomical structures. An expanded VGA method was described by Båth and Månsson (2007) due to the often incorrect use of statistical methods when analysing visual grading data. The method is termed visual grading characteristic (VGC) analysis and has been used in some studies, e.g., Carlander et al. (2008) and Leander et al. (2010). Another approach is visual grading regression, which is applicable when studying the effect from several factors (e.g. the kV and mAs settings) at once (Smedby and Fredrikson, 2010).

2.2.1 Image reconstruction methods

Iterative image reconstruction for CT was briefly described in section 2.1.4. This section will describe the image reconstruction methods used for SPECT, but the principles of the iterative reconstruction procedures are also applicable to CT and PET.

SPECT images are reconstructed from projection data acquired using rotating gamma cameras. The technique used to reconstruct the images is based on either analytical or iterative methods (Bruyant, 2002). The goal of image reconstruction is to determine the three-dimensional distribution of a radiopharmaceutical in the patient. The FBP algorithms are analytical reconstruction methods and have limitations as they rely on several assumptions of the imaging process. Other limitations are the presence of streak artefacts due to the back-projection process and accentuated noise because of the necessary filtering (Tsui and Frey, 2006). The iterative algorithms may model the emission and detection process better and compensate for image-degrading effects, such as attenuation, scatter, and variation of the spatial resolution with distance between collimator and patient (Groch and Erwin, 2000; Hutton et al., 1997; Vandenberghe et al., 2001).

The term ‘iterative’ may be defined as a computational procedure that is repeated a number of times (iterations) with the aim to approach a desired approximate result.

The output from one iteration is used as input for the next iteration, and the principle is to find a solution using successive estimates. The general process of the iterative reconstruction technique is to start with an initial guess of the activity distribution. By mathematically simulating the SPECT physics, projection data is calculated by forward-projection from the initial guess of the activity distribution and compared to measured projection data. The difference between the calculated and measured projections is used to update the initial guess via back-projection. The procedure is repeated a number of times (iterations) and the image of the activity distribution is updated (Figure 2.4) (Hutton et al., 2006). The difference between the calculated and measured projection data will decrease, i.e. the reconstruction converges and then diverges to noise because the difference between the calculated and measured projection data is a function of image noise (Hutton et al., 1997). The convergence speed is dependent on the size of the objects and the total number of counts (Liow and Strother, 1993). A number of different iterative reconstruction techniques are available, but the most well-known is maximum likelihood expectation maximisation (MLEM) (Lange and Carson, 1984; Shepp and Vardi, 1982).

To improve the speed of iterative reconstruction algorithms, a common applied technique is the accelerated version of MLEM: ordered subsets expectation maximisation (OSEM) (Hudson and Larkin, 1994). Variants of the OSEM algorithm is the most widely used reconstruction method in clinical practise today (Hutton et al., 2006). In OSEM the initial guess is updated after comparison with a subset of projection data. One iteration is completed when all of the subsets have been

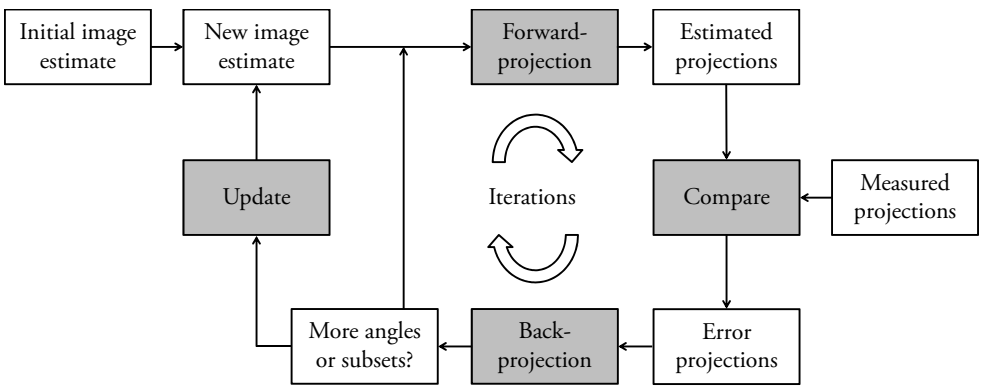

Figure 2.4 Schematic representation of the iterative process used in the reconstruction of SPECT images. The start is an initial estimate of the activity distribution, which after forward-projection is compared to the measured projections. The difference between the estimated and measured projections is via back-projection used to update the initial estimate and this becomes the starting point for the next iteration.

processed. A trade-off exists between contrast/resolution and noise as the number of subsets times the number of iterations (equivalent iterations; EI) increases. Noise increases as the number of subsets and iterations increases. The effect over noise is additive; thus, it is possible to define the EI (Brambilla et al., 2005). Noise amplification can be avoided by early termination of the algorithm (using fewer EI) or by smoothing the images with a reconstruction filter (Beekman et al., 1998). The drawback is a loss of resolution.

3. Material and methods

3.1 Characterisation of radiation dose in CT

The absorbed dose in CT can be characterised in several ways. Effective dose has been estimated based on the DLP. Furthermore, estimates of organ-specific absorbed doses and effective dose have been calculated using Monte Carlo software, as presented below.

3.1.1 Evaluation of radiation dose

In **Papers Ia** and **Ib**, an anthropomorphic chest phantom PBU-X-21 (Kyoto Kagaku, Kyoto, Japan) was used to simulate a patient undergoing a CT thorax examination (Figure 3.1). More information about the phantom is presented in section 3.3.1. CT scans using 16- and 64-slice scanners from four manufacturers (Table 2.2) were performed according to a typical routine adult thorax protocol. The AEC systems were activated and inactivated (scanned with fixed tube current).

In **Paper Ib**, different combinations of adaptation strengths of the CARE Dose 4D AEC system (Kalra and Brady, 2006) were evaluated. From the localisation radiograph, the algorithm determines whether the sections of the patient are slim or obese relative to the internally stored reference patient. On the basis of the pre-selected adaptation strengths, the tube current is decreased for slim sections and increased for obese sections by varying degrees ('weak', 'average' or 'strong') (Figure 3.2).

Figure 3.1 Anthropomorphic chest phantom PBU-X-21 (Kyoto Kagaku, Kyoto, Japan).

To characterise the dynamics of tube current modulation when using an AEC system, the mean mAs value for each reconstructed image slice was plotted for the slice number (**Paper Ia** and **Ib**), making it possible to study how the tube current varied along the z-axis of the anthropomorphic chest phantom.

$CTDI_{vol}$ and DLP were obtained for each CT scan from the digital imaging and communications in medicine (DICOM) image information. In **Papers Ia** and **Ib**, the differences in DLP and $CTDI_{vol}$, respectively, were calculated using and without using the AEC. The difference was presented as an estimation of the percentage dose reduction obtained by using the AEC system.

In **Papers II** and **IIIa**, the effective dose was estimated from the recorded DLP for each scan using Equation 2.5. Conversion factors for the region-specific DLP to effective dose were obtained from Huda et al. (2004) and Bongartz et al. (2004), respectively.

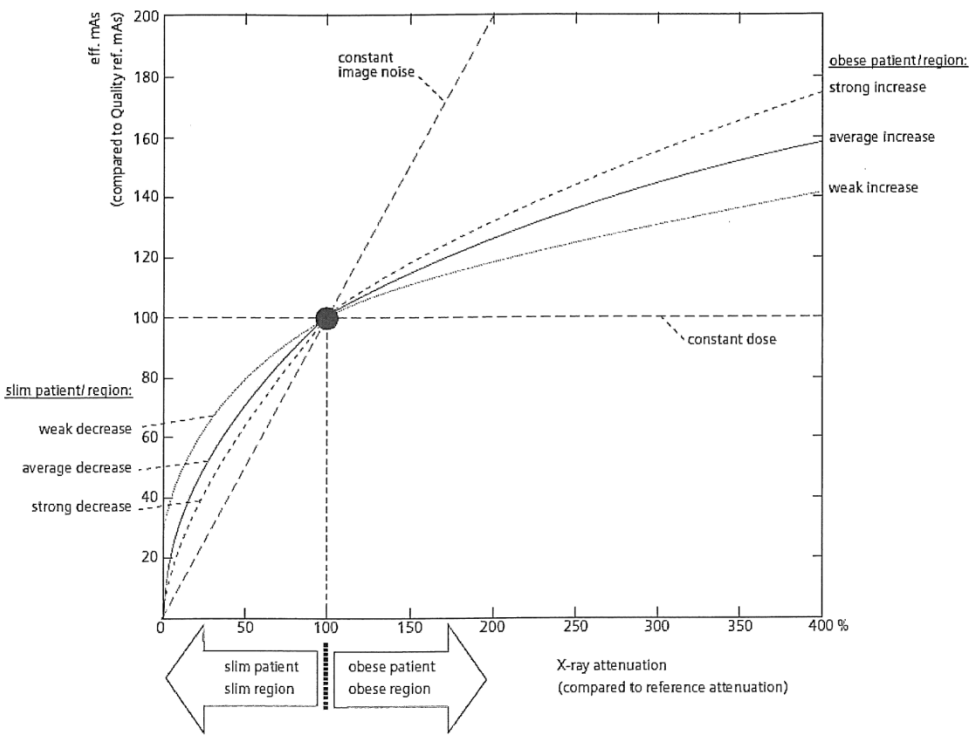

Figure 3.2 Illustration of the adaptation strengths in relation to relative attenuation and relative tube current. The left branch shows the optional adaptation strengths for slim regions, and the right branch shows the optional adaptation strengths for obese regions. Reproduced from Kalra and Brady (2006) with permission from Siemens Medical Solutions (Forchheim, Germany).

The PCXMC software

In **Papers IIIa** and **IIIb**, organ doses and effective dose to the patient using a cone-beam O-arm imaging system (Medtronic, Littleton, USA) (Figure 3.3) in spinal surgery were estimated. The main purpose of using the O-arm system during spinal surgery is to delineate the cortical borders of the pedicles, helping the surgeon correctly insert the pedicle screws between the inner and outer pedicular cortex (Figure 3.9). The system is based on a conventional X-ray tube and a flat panel detector (30 cm x 40 cm). In 3D mode the tube-detector assembly rotates 360° in 13 seconds and a total of 192 axial images are reconstructed with a slice thickness of 0.83 mm, and with a beam-on time of 3.91 seconds (391 shots each 0.01 second long) (Medtronic, 2010). Because the O-arm system is a CBCT, the dose assessment software available for conventional CT is not usable. In addition, the CTDI quantity is not appropriate because the beam width exceeds 100 mm. Instead, a Monte Carlo program for calculating patient doses in medical X-ray examinations was used: PCXMC 2.0 (Tapiovaara and Siiskonen, 2008).

The absorbed dose to selected radiosensitive organs (bone marrow, breast, colon, oesophagus, gonads, liver, lungs, stomach, and thyroid) and effective dose were calculated using a mathematically simulated hermaphrodite phantom. The size of the phantom was selected to correspond to a 15-year-old patient (168.1 cm/56.3 kg) because the majority of patients are adolescents. The exterior shape of the phantom trunk is an elliptic cylinder (thickness 19.6 cm, width including arms 34.5 cm). The available phantoms in PCXMC are based on the mathematical phantoms described by Cristy and Eckerman (1987). Five different scan settings were investigated:

Figure 3.3 The O-arm with telescoping gantry section, which enables lateral patient access. Reproduced from Medtronic (2009) with permission from Medtronic (Littleton, USA).

two were recommended by the O-arm manufacturer (large patient: 120 kV/320 mAs and small patient: 120 kV/128 mAs) (F.X. Massé Associates Inc, Gloucester, USA, 2009), and three low-dose settings (80 kV/80 mAs, 80 kV/40 mAs, 60 kV/40 mAs). For the Monte Carlo calculations, the geometry of the examination, the X-ray spectrum (tube voltage, anode angle, and filtration), and input exposure parameters in terms of tube current-time product were specified. Radiation doses were obtained every 30° (12 projections) of the X-ray tube projection angle, which was intended to simulate the tube rotating around the patient, at two regions: thoracic spine and lumbar spine (Figure 3.4).

The resulting organ doses and effective dose of the entire examination were obtained by summation of the contributions from each projection angle. The effect of changing the number of simulated projection angles (24, 12, and 4) on effective dose was investigated (**Paper IIIa**). Each projection was simulated using 1×10^6 photons, resulting in ~0.1% stochastic uncertainty in the effective dose from the Monte Carlo simulation. The effective dose was calculated using tissue-weighting factors from ICRP Publication 60 (1991) and ICRP Publication 103 (2007b).

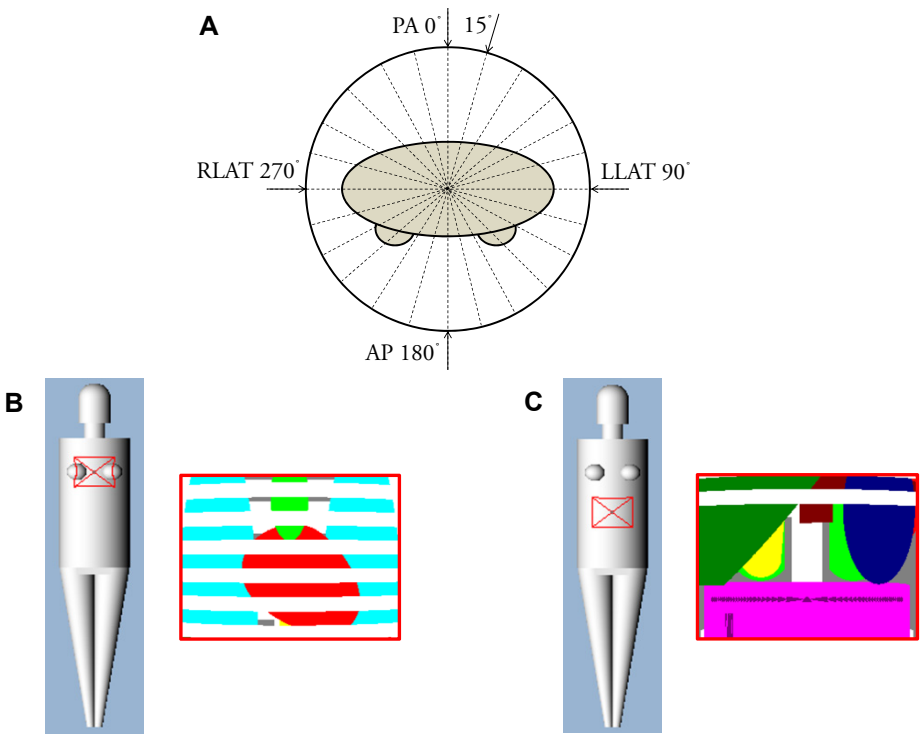

Figure 3.4 Axial view of the phantom showing projections obtained every 15° (30° in **Paper IIIb**) of the X-ray tube projection angle (A). Coronal view of the phantom taken from the PCXMC software, showing the anteroposterior projection (180°) and location of organs in the X-ray field at the two investigated regions: thoracic spine (B) and lumbar spine (C).

3.1.2 Radiation dose versus amount of contrast medium

In **Paper II** following relationship between quantum noise and radiation absorbed dose was used: quantum noise is inversely related to the square root of the tube load (mAs), which is directly related to the radiation dose. Thus, reduction of tube load in a CT protocol leads to an increase in image noise. In abdominal CT, diagnosis of the majority of pathological entities relies on CM use. A higher amount of CM will increase the contrast of the tissue and organs as the CM courses through them. Therefore, theoretically, balancing noise and image contrast against each other is possible by varying tube load and the amount of CM, respectively, maintaining a constant CNR. A similar idea was evaluated by Watanabe et al. (2010).

Based on the theoretical model described in Figure 3.5, 100 patients were consecutively divided into four age groups. The model can be likened to a seesaw balancing the radiation absorbed dose (quality reference mAs) and the amount of i.v. CM. As a starting point for the model, the abdominal CT protocol formerly used at the department was used (200 quality reference mAs and 420 mg I kg^{-1}). The quality reference mAs and amount of CM was selected to maintain CNR for the four groups. The resulting parameters are shown in Table 3.1.

Since adipose tissue is poorly perfused it may be an advantage if the amount of CM is adapted to the lean body weight (Kondo et al. 2010). For this reason the amount of CM in the evaluated protocol was linearly proportional to body weight up to 75 kg. To keep the number of variables at minimum when evaluating the theoretical model behind the protocol, patients with body weight exceeding 75 kg were excluded from the study.

Table 3.1 CT parameters for the four age groups. Group III, which was investigated using the formerly used protocol was used as a reference group. Twenty-five weight-matched patients were included in the study for each group.

Patient group	Patient age (years)	Quality reference mAs	CM dose (mg I kg^{-1})
Group I	16-25	100	600
Group II	26-50	150	500
Group III	51-75	200	420
Group IV	>75	300	350

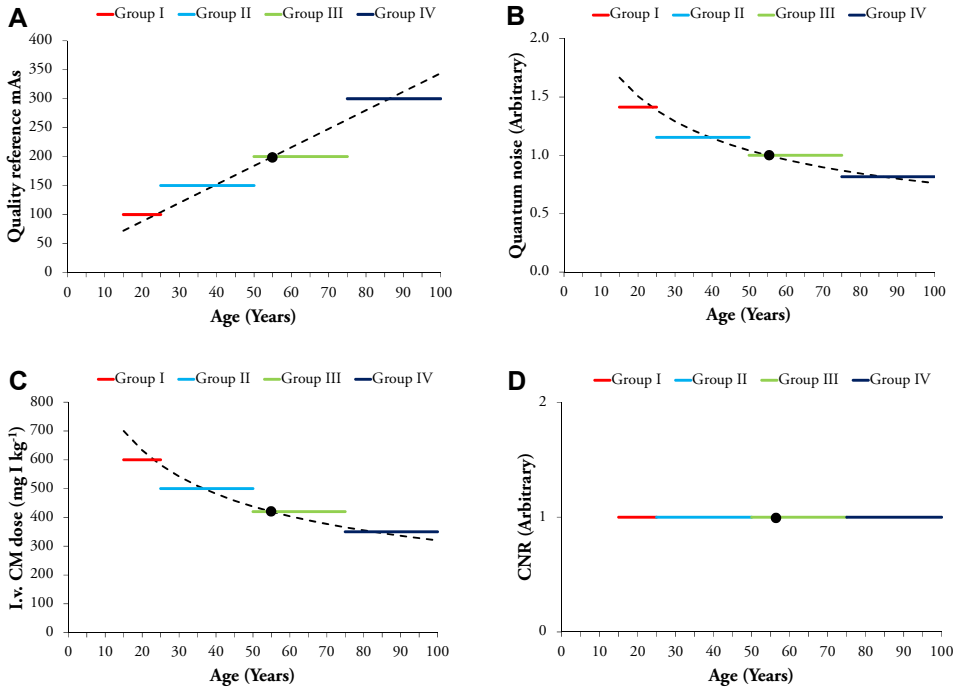

Figure 3.5 Theoretical model behind the selection of examination parameters for the new protocol likened to a seesaw balancing radiation absorbed dose and i.v. CM dose. The black dot represents the formerly used protocol: 200 quality reference mAs and 420 mg I kg^{-1} (group III). Quality reference mAs was plotted in a linear relation to patient age, indicated by the dashed line (A). The resulting arbitrary quantum noise, which is inversely proportional to the square root of quality reference mAs was calculated, indicated by the dashed curve (B). To compensate for the variation in image noise, the amount of i.v. CM was plotted to match the noise curve, indicated by the dashed curve (C). Theoretically, this will result in a constant CNR for all ages (D). Four patient age groups were selected based on the model, indicated by the horizontal lines (A-D).

3.2 Characterisation of radiation dose in SPECT and PET

Absorbed dose to various organs and tissues and the effective dose were determined using tables of absorbed dose coefficients and effective dose coefficients given by the ICRP (1988; 1998; 2008). In **Paper V**, the patients were referred for the detection of neuroendocrine tumours, such as pheochromocytomas or neuroblastomas, and their metastases. These tumours commonly occur in the abdomen or the adrenal glands. SPECT acquisitions were performed 4 h and 24 h after the injection of approximately

200 MBq ^{123}I-MIBG. MIBG is a pharmaceutical with high uptake in both normal sympathetically innervated tissues (e.g., heart and salivary glands) and abnormal tissues (tumours of neuroendocrine origin associated with the expression of neurohormone transporters) (Vallabhajosula and Nikolopoulou, 2011). The effective dose for the ^{123}I-MIBG-SPECT examinations was estimated. According to ICRP (1998), the effective dose per unit of administered activity for adults is 0.013 mSv MBq^{-1}.

3.3 Evaluation of image quality

There are several ways to evaluate image quality in medical imaging systems. Objective evaluations of patient and phantom images were performed as presented below. Different observer performance studies evaluating images of patients and a cadaveric pig spine were also performed (section 3.3.2).

3.3.1 Objective evaluation

In **Paper II**, patient images were objectively evaluated by determining the SNR and CNR in the liver (Figure 3.6). The attenuation (signal) was measured by placing a circular ROI with a diameter of approximately 3 cm in a homogenous part of the right liver lobe, avoiding vascular and biliary structures. The SD was used as a measure of the image noise and the liver SNR was calculated. To calculate the CNR, the difference in attenuation between the measured value in the liver and a hypothetical hypovascular liver metastasis with attenuation of 40 HU was used as contrast and then divided by the noise value. Liver metastases often have a slightly lower attenuation than normal liver parenchyma, are typically hypovascular, and not enhanced by i.v. CM in the portal venous phase (Figure 3.7) (Heiken et al., 2006; Kanematsu et al., 2006).

Anthropomorphic chest phantom

In **Papers Ia**, **Ib**, and **IIIb**, anthropomorphic chest phantom PBU-X-21 (Kyoto Kagaku, Kyoto, Japan), which closely resembles a human chest, was used to simulate a patient (typically lean Asian male). The skeleton in this phantom is made to resemble a skeleton of a 160-cm tall male and consists of epoxy resins, calcium hydroxyapatite, and other substances to achieve variations in contrast in the phantom images similar to those of a human body. The remainder of the phantom is made of urethane, which resembles soft tissue. The phantom also contains material that simulates blood vessels, including pulmonary capillaries.

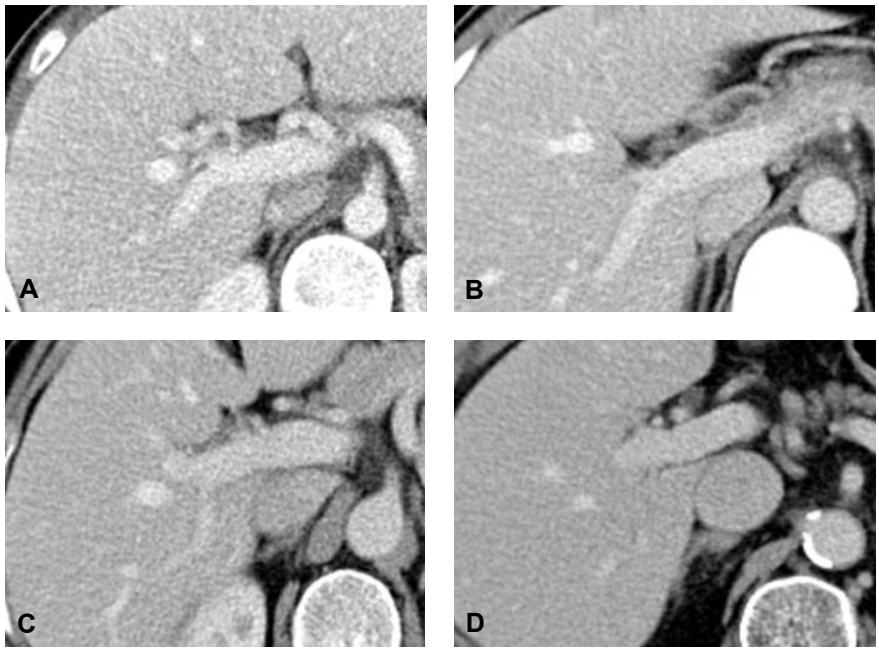

Figure 3.6 Examples of CT images of the liver in the four age groups: group I (A), group II (B), group III (C), and group IV (D) (**Paper II**).

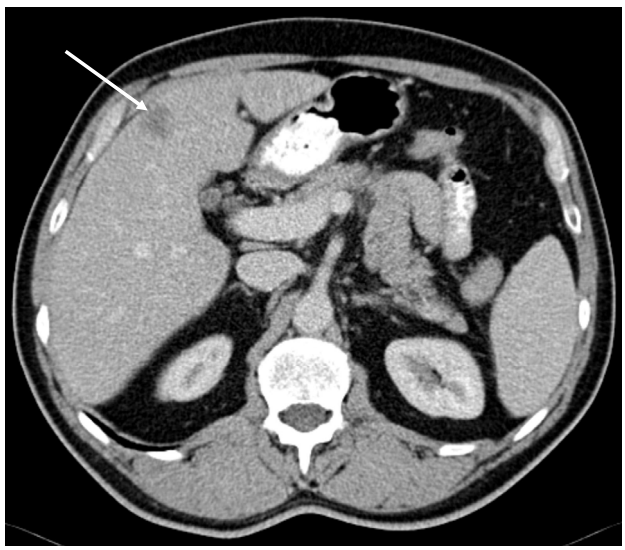

Figure 3.7 Hypovascular liver metastasis in a 60-year-old man. The liver parenchyma (82 HU) is enhanced by the i.v. CM in the portal venous phase and the metastasis (41 HU) is sparsely filled with CM. The patient was examined using the parameters for group III (200 quality reference mAs and 420 mg I kg^{-1}).

To evaluate how the AEC systems affected image quality, the image noise values from scans performed with an activated AEC system were compared to those obtained without AEC (**Papers Ia** and **Ib**). Circular ROIs of 0.5 cm^2 were placed in the vertebral foramen of the chest phantom because this region is uniform and available throughout the phantom (Figure 3.8). The SD of the CT number was used as a measure of the image noise. To evaluate whether the image noise became more uniform when using the AEC system, the coefficient of variation (C_v) expressed as a percentage was calculated (**Paper Ia**):

$$C_v = \frac{\sigma}{M} \cdot 100 \tag{3.1}$$

where M is the mean value of the measured image noise values in the vertebral foramen throughout the chest phantom and σ is the calculated SD of the measured image noise values.

In **Paper IIIb**, the chest phantom was examined on the O-arm system using different scan settings: two recommended by the O-arm manufacturer (120 kV/320 mAs and 120 kV/128 mAs) (F.X. Massé Associates Inc, Gloucester, USA, 2009), and three low dose settings (80 kV/80 mAs, 80 kV/40 mAs, 60 kV/40 mAs). The pedicular width was independently measured by two readers at seven thoracic and four lumbar vertebrae (a total of 22 pedicles, 11 on each side). The pedicular width was measured at the widest and narrowest part of every individual pedicle (44 measurements per reader per scan) (Figure 3.9). The measure of the pedicle width at the narrowest part is routinely used to determine the screw diameter.

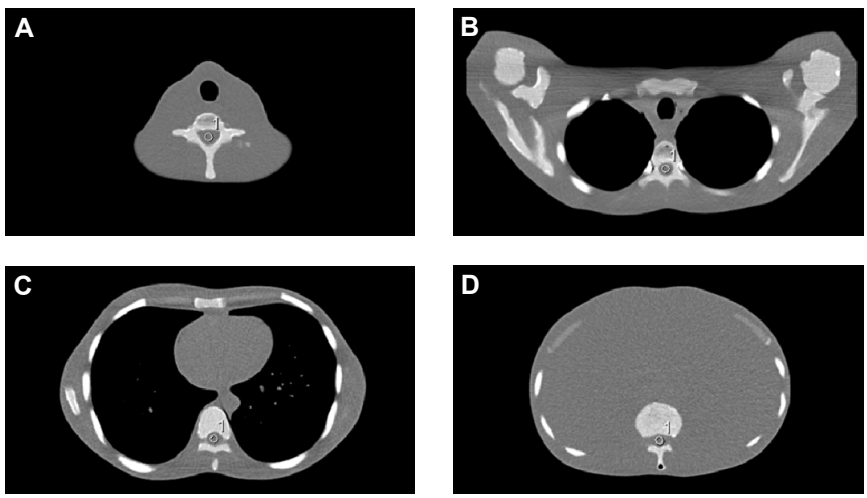

Figure 3.8 Cross-sectional views showing ROI placement in the vertebral foramen of the anthropomorphic chest phantom: slice 10 (A), slice 25 (B), slice 50 (C), and slice 75 (D) (**Papers Ia** and **Ib**).

Figure 3.9 The figure illustrates the method for measuring the pedicular width. In the axial image the pedicular width is defined as the distance between point A and B (**Paper IIIb**).

The MADEIRA SPECT- and PET-phantom

The majority of phantoms used to characterise a SPECT or PET system are built by cylinders containing fillable inserts, phantoms consisting of multiple discrete disks or sheets, or tissue-equivalent anthropomorphic phantoms. In a European Commission research project named MADEIRA (minimising activity and dose with enhanced image quality by radiopharmaceutical administration) (Hoeschen et al., 2010), a new patent-filed phantom (European patent application no. 09008184, "Phantom for a tomographic medical imaging apparatus"), the 'MADEIRA' phantom, was designed. Using this phantom, different target to background activity ratios can be provided simultaneously with a linearly changing diameter of active or inactive lesions.

The phantom described in **Paper IV** has an external vessel with a half-cylindrical outline that allows it to be incorporated into the anthropomorphic RSD Alderson heart/thorax phantom (Radiology Support Devices, Long Beach, USA) (Figure 4.6 A). The MADEIRA phantom itself contains 16 cones with a linearly decreasing inner diameter over a length of 19 cm, from 16 mm to 2 mm (Figure 3.10). The wall thickness of the cones is 1 mm. The 16 cones are separately fillable with activity in water solution, as is the outer vessel. The phantom is constructed of acrylic glass for visual inspection of bubble-free filling.

In **Paper IV** the 16 cones were filled with ^{99m}Tc- and ^{18}F-solutions of different activity concentrations differing by a factor of ¾ from cone to cone, and acquisitions were performed using a Symbia T2 SPECT/CT (Siemens Medical Solutions, Forchheim, Germany) and Gemini 16 PET/CT (Philips Healthcare, Best, The Netherlands), respectively. The lowest relative activity concentration was 0.1 and the highest 10, where 1 refers to the background activity concentration in the external vessel.

A measure of the spatial resolution evaluated as the full width at half maximum can be obtained by drawing a profile across the centre of the cones. PVE was evaluated by

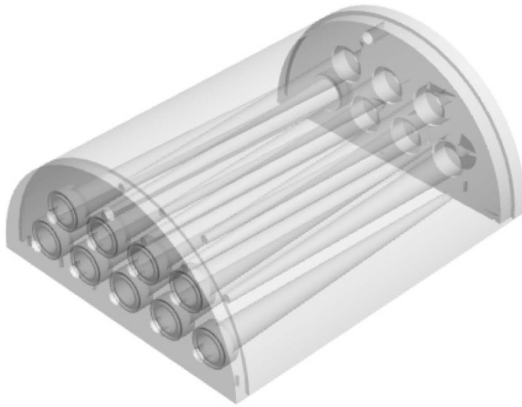

Figure 3.10 The construction of the MADEIRA phantom used in **Paper IV**. Courtesy of U Engeland (Scivis GmbH, Göttingen, Germany).

drawing profiles in the centre along the length of the cones. Detectability can be evaluated subjectively using the visibilities of the cones as a function of the diameter of the cones, corresponding to lesions of different sizes. In addition, detectability can be evaluated objectively by determining the contrast as the difference in number of counts in the cones and in the background using ROIs.

3.3.2 Subjective evaluation

The methods used for subjective evaluations presented in this thesis are different types of visual-grading, observer performance studies, performed both absolutely and relatively as presented below.

Absolute analysis

In **Paper IIIb**, anthropomorphic chest phantom images examined on the O-arm system with scan settings described in section 3.3.1 were independently evaluated by two experienced observers, both radiologists. The images were presented in consecutive order, lowest exposure parameters first, and all evaluations were performed in the picture archiving and communication system (PACS; Sectra AB, Linköping, Sweden). The task of the observers was to subjectively rate the reproduction or visibility of a certain structure. Four criteria from the European guidelines on quality criteria for CT were used (Bongartz et al., 1999):

1. Visually sharp reproduction of the cortical and trabecular bone
2. Visually sharp reproduction of the intervertebral joints
3. Visually sharp reproduction of the intervertebral disk profiles
4. Visually sharp reproduction of the intervertebral radicular canals

The criteria in every individual scan were graded as: 'reliable', 'relatively reliable', or 'unreliable'.

To evaluate the impact of streak artefacts induced by metal implants, a cadaveric pig spine from a 50-kg pig was used. A total of 20 pedicle screws at 10 consecutive vertebral levels (6 thoracic and 4 lumbar) were inserted. The cadaveric pig spine was examined using the O-arm with the same scan settings as for the chest phantom. Two observers were asked to:

1. Grade the images with regard to their reliability of assessing the screw position as reliable, relatively reliable, or unreliable.
2. Grade the screw placement into 'normal placement' when the screw is enclosed within the pedicle or minimally violates the pedicular cortex, or 'misplacement' when more than half of the screw diameter violated the pedicular cortex (Figure 4.4 G and H).

For comparison, the cadaveric pig spine was examined using conventional CT. Two CT protocols were used: (a) 120 kV/320 mAs and (b) low-dose CT with 80 kV/25 mAs. Reconstructed 1-mm-thick slices were used to evaluate screw placement.

Visual grading characteristic analysis

In **Paper II** the image quality obtained for patients given in Table 3.1 was evaluated using VGC analysis (Båth and Månsson, 2007). Seven criteria from the European guidelines on quality criteria for CT were used (Bongartz et al., 1999):

1. Visually sharp reproduction of the liver parenchyma and intrahepatic portal veins
2. Visually sharp reproduction of the pancreatic contours
3. Visually sharp reproduction of the kidneys and proximal ureters
4. Reproduction of the gallbladder wall
5. Visually sharp reproduction of the right adrenal gland from adjacent structures
6. Visually sharp reproduction of the structures of the liver hilus
7. Reproduction of the ductus choledocus in the pancreatic parenchyma

All criteria were judged absolutely using a 5-grade scale: (1) unacceptable, (2) substandard, (3) acceptable, (4) above average, or (5) superior. A sixth alternative 'not applicable' could be used for criteria 4 if the gallbladder was removed and the data were excluded from further analysis.

The images were presented and evaluated using the software ViewDEX (Viewer for Digital Evaluation of X-ray images) (Håkansson et al., 2010) in one of the department's regular PACS workstations. All images were viewed individually by four observers, all radiologists. The information on patient identity and scanning parameters were removed and the images were presented in random order to each observer.

The rating data was analysed using methodology developed in ROC analysis. A VGC curve was obtained by plotting the cumulative distributions of rating data for two systems compared against each other (Båth and Månsson, 2007). The area under the VGC curve (AUC_{VGC}) was used as a measure of the difference in image quality between the two systems. An AUC_{VGC} of 0.5 corresponded to equal image quality in the two systems, an $AUC_{VGC}<0.5$ indicated that the image quality was higher for the reference system, and an $AUC_{VGC}>0.5$ indicated that the image quality was higher for the evaluated system.

As the parameters used for group III (Table 3.1) were the same as in the formerly used protocol, this group was selected as the reference for the VGC analyses. Calculations comparing groups I, II, and IV to group III were performed individually for all seven criteria and the readers assembled, using the recently developed software for multiple observers: VGC Analyzer (M Båth and J Hansson, The Sahlgrenska Academy at University of Gothenburg). If the 95% confidence interval for the estimation of AUC_{VGC} did not include the value 0.5, a statistically significant difference at the 95% level between the two evaluated systems was established.

VGC analysis only provides information about the image quality in relation to another group and not about the absolute level of image quality. Calculating mean values for the grades would be not be appropriate because they are ordinal data; therefore, the percentage of grades in each group rated 'acceptable' or better (grades 3, 4, and 5) was used as a measurement of the absolute level of image quality.

Rank-order study

ROC studies or derivatives thereof are widely used in medical X-ray imaging to define differences in imaging procedures, but ROC studies are time-consuming, require a large patient cohort with normal and pathological subjects, and the truth needs to be known for each case. No current image quality criteria are established for nuclear medicine examinations as there are for X-ray images. However, if the diagnostic performances are comparable or the differences are small, performing a side-by-side review (rank-order study) may be desirable (Good et al., 1999, Towers et al., 2000). Fewer optimisation trials have been performed in the form of observer performance studies for nuclear medicine imaging compared to X-ray imaging.

In **Paper V** the number of equivalent iterations (EI) was optimised for the Flash 3D (Siemens Medical Solutions, Forchheim, Germany) (Hawman et al., 2003) reconstruction algorithm and compared to two recently developed reconstruction algorithms, ReSPECT (Scivis GmbH, Göttingen, Germany) (Scivis, 2006) and orthogonal polynomial expansion on disc (OPED) (Tischenko et al., 2010; Xu et al., 2007) for application on ^{123}I-MIBG-SPECT. Flash 3D and ReSPECT are iterative algorithms based on the OSEM technique and OPED is an analytic algorithm.

A rank-order study was performed and the SPECT images were interpreted by three experienced observers, all nuclear medicine physicians, by showing the image sets in the software package Scientific Visualizer (Scivis GmbH, Göttingen, Germany) installed on one of the department's regular PACS-workstations. Scientific Visualizer was developed within the MADEIRA project (Hoeschen et al., 2010). The software was adapted for observer studies with the possibility of showing up to eight unlabeled image sets side-by-side. Eleven patients underwent SPECT 4 h after intravenous injection of approximately 200 MBq and 14 patients 24 h post-injection (p.i.). The SPECT data for each patient were presented side-by-side in sagittal, coronal, and transversal views and as a maximum intensity projection in random order and unlabeled. The images were presented in a black and white scale and the observers were free to change the window level settings. No time limit was imposed on the observer's evaluation.

In the first visual assessment, images reconstructed at eight different EI numbers for Flash 3D were displayed (8, 16, 32, 64, 80, 96, 128, and 256 EI). Three observers were asked to rank the three best image sets according to their overall impression of the image quality with regard to noise level, ability to discriminate uptakes in anatomical structures (e.g., liver, adrenal glands, kidneys, and spleen), introduction of artefacts, and if possible delineation of suspected pathology. The rank order was 1 (best) to 3 and the remaining image sets obtained a rank order of 4. This procedure was performed for images acquired 4 h and 24 h after injection. The average distribution of image quality ranking for all observers was calculated for the different EI numbers. In addition, the rank order was obtained based on the calculated average of scores a given image set received, i.e. the lower the value the better the image.

In the second visual assessment, the two best considered EI numbers for Flash 3D were compared to ReSPECT and OPED (Figure 4.7). In the same manner as the first assessment, the observers were asked to rank the image sets according to their overall impression of the image quality. A rank order of 1 was assigned to the image set judged to have the best overall image quality, and a rank of 4 was assigned to the worst. The same procedure was performed for images acquired 4 h and 24 h after injection. The average distribution of image quality ranking for all observers was calculated for the different reconstruction methods. In addition, the rank order was obtained based on the calculated average of scores that a given image set received.

4. Results and discussion

4.1 AEC in CT

A clinical CT examination often covers different anatomic regions with variable attenuation. Because the selected tube current normally is based on the region with the highest attenuation, such as the shoulder and pelvis, or the region that requires the highest image quality, the tube current is usually set to a high level when an AEC system is not used. Standard protocols are usually established to generate good quality images for average patient sizes. Thus, if an AEC system is not used, smaller patients will be exposed to unnecessarily high doses of radiation and images of larger patients may be of lower quality. AEC systems were developed to enable tube current modulation according to a patient's size, shape, and attenuation, and to improve the consistency of image quality among patients.

4.1.1 Evaluation of AEC systems

There are a number of benefits to using an AEC system. One benefit is the potential for dose reduction, as shown in **Paper Ia**. For the anthropomorphic chest phantom, the magnitude of the reduction in absorbed dose was considerable, ranging from 35% to 60%. It is difficult to compare the estimated dose reduction obtained in this study with the values reported in the literature. The results are strongly dependent on the selected scanning parameters, the CT scanner/model, and the specified image quality for the AEC system. However, good agreement was found with several other studies, e.g., Mulkens et al. (2005) and Rizzo et al. (2006) who studied patient populations. Gutierrez et al. (2007) and Papadakis et al. (2008) also found similar dose reductions with anthropomorphic phantoms.

Because the calculated reduction in radiation absorbed dose is based on the selected mAs value when the AEC systems are inactivated and on the level of required image quality (Table 2.2), it is crucial that these values are representative for a clinical thorax CT protocol. The result should be interpreted as an indication of a potential for reducing radiation dose. A recent study by Papadakis et al. (2011) showed that the calculated dose reduction based on the average tube current used throughout the scan, i.e. $CTDI_{vol}$ and DLP, disagrees with the estimated reduction in the effective dose based on organ dose measurements with thermoluminescent dosimeters. The study found 41% (underestimation) and 2.6% (overestimation) differences for a thorax scan and abdomen-pelvis scan, respectively, using an adult anthropomorphic phantom.

As shown in **Paper Ia**, the dynamics of tube current modulation for each of the AEC systems were similar, especially between GE and Toshiba and between Philips and Siemens AEC systems (Figure 4.1). The variation in image noise among images obtained along the scanning direction was lower when using the AEC systems compared to the scans with fixed mAs, especially for GE and Toshiba systems. Use of the AEC systems, in general, increased the image noise measured in the vertebral foramen of the chest phantom (Figure 5 and 6 in **Paper Ia**).

The different AEC systems were designed for different purposes. Two different approaches are currently used: 'constant noise systems' (GE and Toshiba) and 'adequate noise systems' (Philips and Siemens). GE and Toshiba claim that their systems were designed to increase the uniformity of image quality between different anatomical regions in the same patient. The basis for the Siemens AEC system is that different sized patients require different levels of noise in order to obtain adequate image quality (Figure 3.2). In slim patients, lower noise levels are desired, whereas more noise is often acceptable in obese patients because they contain more fat as an intrinsic contrast agent. The user can also control the extent of the tube current adjustment for slim and obese patient sections by selecting weak, average, or strong adaptation strengths (evaluated in **Paper Ib**, section 4.1.2). The Philips AEC system, Automatic current selection (ACS), uses the same approach as Siemens; more noise is accepted for obese patients and less noise is required for small patients.

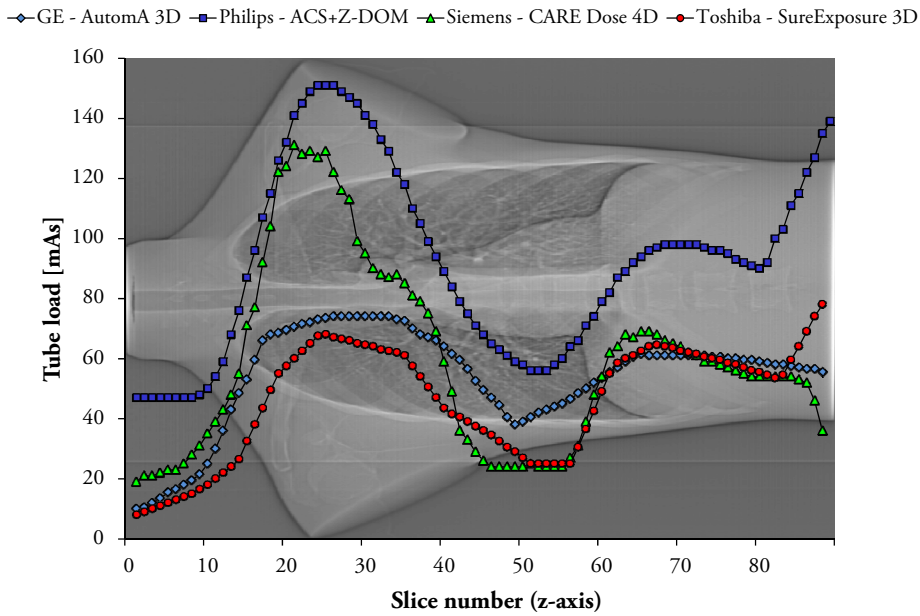

Figure 4.1 Mean mAs values along the longitudinal axis of the chest phantom for each manufacturer on their respective 64-slice CT scanner overlaid on the scan projection radiograph. Philips and Siemens report mAs as mAs/pitch.

Whether the diagnostic accuracy was influenced by the AEC-induced increases in image noise was not evaluated in **Papers Ia** and **Ib**. A subjective clinical image quality analysis performed by Rizzo et al. (2006) showed that the image noise was significantly higher in examinations performed with combined modulation (CARE Dose 4D) compared to a fixed tube current. However, the study also concluded that the diagnostic utility of the images was acceptable.

From a user perspective, AEC systems may appear as 'black boxes' due to insufficient information regarding the operating method. Nagel et al. (2011) pointed out the need for increased specifications of AEC systems and showed that simple tests with quality control phantoms allow more detailed insight into the characteristics and limitations of an AEC system.

AEC systems have several limitations and pitfalls. An AEC system will not automatically decrease the radiation dose to the patient. The adaptation of patient exposure is dependent on the user-specified image quality and patient size. To maintain constant image quality between different patient sizes, the AEC system can lead to an increased radiation dose for larger or obese patients. The response of AEC systems to variation in the scan and reconstruction parameters is different between manufacturers (Keat, 2005). The adaptation of tube current in regions with high-attenuated metal implants is also different (Dalal et al., 2005). The localisation radiograph is fundamental for an AEC system because the system determines the adequate tube current level from the localiser. Therefore, to ensure optimal image quality and minimal radiation dose, it is important that the patient is at the same position for the localisation and subsequent scan, localisation is sufficiently long, the patient is always positioned in the centre of the scan field, and if using protective devices, such as bismuth shielding, it is applied after the localisation (Singh et al., 2011).

4.1.2 The effect of different adaptation strengths

Paper Ib shows that, for the anthropomorphic chest phantom, it was possible to reduce the absorbed dose using CARE Dose 4D to 50% compared to the constant tube current technique. The degree of reduced absorbed dose depends on which adaptation strength setting is used (27-52% and 28-50% for Sensation 16 and Sensation 64, respectively). Accordingly, the difference in the dose reduction between the setting strong/weak and weak/strong was >20%. A substantial difference in image quality (image noise) was observed between the adaptation strengths. Independent of selected adaptation strengths, a significant increase in image noise was seen throughout the chest phantom compared to the constant tube current technique (Figure 3 in **Paper Ib**). The results are in agreement with those of Papadakis et al. (2008), who found a dose reduction of 45% in the thorax and abdomen region (average/average) using an adult anthropomorphic phantom. The prior study also

found significantly increased image noise and significantly decreased SNR compared to fixed tube current.

As shown in **Paper Ib**, the adaptation strengths can be used to obtain user-specified modifications of image quality or absorbed dose to the patient. Radiologists and medical physicists need to be aware of the differences between different adaptation strengths, and such differences are useful when attempting strategies to optimise CT radiation dose. In the latest version (VA40) of CARE Dose 4D, the adaptation strengths can be specified separately for each body region. The strengths have also been expanded, and it is now possible to choose 'very weak' and 'very strong'. Separate adaptation settings are also available for adult and child protocols, and child protocols use the adult reference patient (75 kg).

4.2 Balancing radiation dose and amount of contrast medium

The abdominal CT protocol evaluated in **Paper II** reduced the mean effective dose for group I (3.6 mSv) by 57% and by 22% for group II (6.6 mSv), but it was increased by 46% for group IV (12.4 mSv), compared to formerly used parameters in group III (8.5 mSv). For elderly patients, the amount of i.v. CM was reduced by 18%. Thus, the most important risk for each group was reduced.

The objective evaluation (section 3.3.1) in terms of the mean SNR in the liver in groups I-IV ranged from 7.3 (group II) to 8.4 (group IV). The mean CNR-values for a hypothetical hypovascular liver metastasis ranged from 4.3 (group III) to 5.1 (group I). Analysis with ANOVA and Tukey's multiple comparison test could not establish significant differences in SNR and CNR between the groups.

The result from the VGC analysis (section 3.3.2) is presented in Figure 4.2. For group I and group II the AUC_{VGC}-values indicated significantly lower subjective image quality for four and one of the seven criteria, respectively, compared to group III. No significant difference was found between groups III and IV. The proportion of grades 'acceptable' or better (grades 3, 4, and 5) was 71% for group I, 80% for group II, 85% for group III, and 83% for group IV.

The discrepancy between objective and subjective image quality in this study is of interest and needs to be analysed further. One explanation for the discrepancy may simply be that the noise level was too high in the low radiation groups. The discrepancy may also reflect a weakness in the method, as reproduction of normal structures may not be affected by image noise in a way that is directly comparable to the conspicuity of low contrast lesions. The theory behind the protocol is that increased noise is compensated for by increased lesion contrast, and this may not be applicable to the anatomical structures that are rated. An assumption with VGC

analysis is that a correlation exists between the reproduction of anatomy and pathology. Yet another explanation is that the readers, from normal practice, were not accustomed to reading high-noise images, thereby rating these images lower.

The study only included patients with body weight up to 75 kg, with the assumption that the additional tissue in patients with body weight over 75 kg mainly consists of adipose tissue and that this tissue has a small vascular and interstitial space and thus contributes little to the dispersing or diluting the CM in the blood (Kondo et al., 2010). The presence of additional adipose tissue can be compensated for by increasing the tube current using the AEC system to get comparable noise level as for 75 kg body weight.

To the author's knowledge, no previous studies have explored this concept of balancing the radiation absorbed dose against the amount of CM in abdominal CT. One recent study by Watanabe et al. (2010) evaluated the idea of increasing the i.v. CM dose to allow for a reduced radiation dose. The study used a slightly different methodology, rating the depiction of vessels using different radiation and CM doses, finding that the qualitative image quality was preserved with a 30% reduced radiation dose compensated by a 15% increase in amount of CM.

The finding that it is possible to compensate for a reduction in absorbed dose by increasing the amount of i.v. CM may represent one additional step in the pursuit of minimising effective dose to young patients. Further developments in the abdomen CT protocol may be to lower the kV for smaller patients in order to achieve higher CNR for the same amount of iodine and to add iterative reconstruction to reduce the noise level in low radiation dose images. In Siemens novel CT systems, CARE kV can be used together with the protocol; consequently, the tube voltage will be adapted individually for each patient to obtain an optimal CNR. Diagnostic performance was not investigated and future work aims to establish sufficient image quality for lesion detection in the liver using dose reduction simulation software (Söderberg et al., 2010).

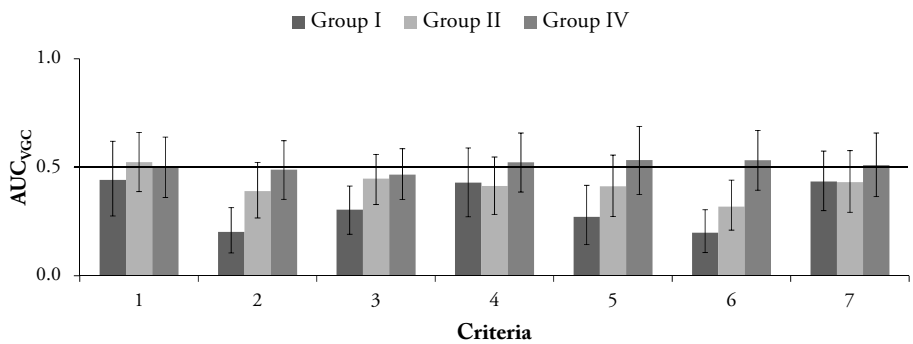

Figure 4.2 The AUC_{VGC}-values per criterion (given in section 3.3.2) for readers assembled. If the confidence interval does not include 0.5, the subjective image quality is significantly different from the reference group (III) at a 95% confidence level.

4.3 Optimisation of the O-arm system

4.3.1 Estimation of organ dose and effective dose

In **Paper IIIa**, the absorbed doses to different organs from spinal surgery using the O-arm imaging system were calculated using the Monte Carlo-based software PCXMC 2.0 (section 3.1.1). The highest estimated absorbed doses were received by the breast and lungs when scanning the thoracic spine, and stomach when scanning the lumbar spine (Figure 4.3). The absorbed dose to the breast was 14 mGy using 120 kV/128 mAs (standard settings recommended by the manufacturer for a small patient) to the thoracic spine. The absorbed dose to the thyroid gland was 7 times higher with the standard scan than in the evaluated low-dose scan (80 kV/80 mAs). Corresponding values for the breasts, stomach, and gonads were 4, 5, and 6 times higher.

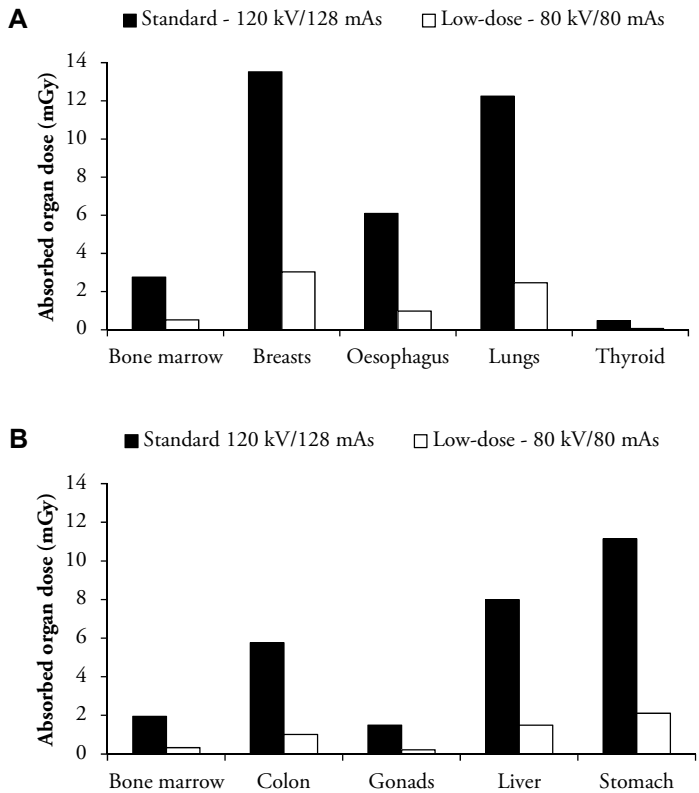

Figure 4.3 Estimated absorbed dose to different organs. The values are the sum of contributions from 24 simulated projection angles for scanning the thoracic spine (A) and lumbar spine (B). The absorbed dose to the gonads is defined as the absorbed dose to the ovaries. The testicular absorbed dose was negligible.

The effective dose for the standard scan was 5 times higher than the dose delivered with the low-dose scan. The useful reconstructed scan length for the O-arm is 15 cm. Consequently, to image the thoracic and lumbar spine, 2-3 scans are often needed per patient during a correction of deformity in scoliosis. This requirement means a total effective dose of 7.9-12 mSv using the scan parameters recommended by the manufacturer. Corresponding scans using low-dose settings result in 1.5-2.4 mSv and represent a considerable reduction in effective dose. The effective dose during fluoroscopy-assisted lumbar spine surgery has been reported to be approximately 2.3 mSv when the X-ray source is positioned superiorly compared to 6.8 mSv in the source-inferior situation (Jones et al., 2000).

The calculated effective dose in the thoracic spine, using tissue-weighting factors from the ICRP publication 103 (2007b), were 28% higher than those calculated with factors from ICRP publication 60 (1991). This difference is explained by the increase in tissue-weighting factor from 0.05 to 0.12 for the breast. The estimated effective dose with PCXMC was similar with the calculated effective dose using conversion factors for DLP to effective dose.

The method used to calculate patient dose for cone beam CT was previously used by He et al. (2010), who investigated how the tube projection angle affects the organ doses and effective dose. In **Paper IIIa**, no difference in effective dose was found when using 24 or 12 projection angles. The effective dose was 35% lower using four projections compared to 24 or 12 projections for the low-dose scan of the lumbar spine. Accordingly, four projection angles every 90° were not enough to accurately simulate the X-ray tube rotating around the patient. Future studies are needed to verify the organ doses estimated by Monte Carlo with absorbed dose measurements in anthropomorphic phantoms.

4.3.2 Optimisation of radiation dose and image quality

The use of the O-arm system has been shown to provide great clinical value for spinal surgery in the form of greater accuracy, a lower rate of screw misplacement, and reduced intra-operative time (Houten et al., 2011; Nottmeier et al., 2009; Santos et al., 2012). A study by Zhang et al. (2009) showed that, with the same radiation dose, the O-arm has high-contrast spatial resolution comparable to a conventional CT system but worse low contrast.

However, as shown in **Paper IIIa**, the O-arm, if operated without optimisation, may deliver high radiation doses; consequently, there is a strong need to optimise the clinical scan protocols, especially because the majority of the patients are adolescents. In **Paper IIIb**, the radiation dose and image quality were evaluated for five different scan settings (Figure 4.4). The effective dose for a 120 kV/320 mAs scan was 13, 26, and 69 times higher than the dose delivered with 80 kV/80 mAs, 80 kV/40 mAs, and 60 kV/40 mAs scans, respectively.

Subjective evaluation (section 3.3.2) of the phantom images showed that images obtained at 60 kV/40 mAs were relatively reliable in the thoracic spine and unreliable in the lumbar spine. The readers graded images obtained at 80 kV/80 mAs and 80 kV/40 mAs as reliable in the thoracic spine and relatively reliable in the lumbar spine. Images obtained using the settings recommended by the manufacturer, 120 kV/128 mAs and 120 kV/320 mAs, were considered reliable by both readers. Images of the cadaveric pig spine operated on with pedicle screws obtained at 60 kV/40 mAs were graded by both observers as unreliable and images obtained at 80 kV/40 mAs as relatively reliable (unreliable in the lumbar spine). Images obtained at 80 kV/80 mAs and 120 kV/128 mAs were graded as reliable.

Images of the cadaveric pig spine obtained at 60 kV/40 mAs were unreliable and measurements of the pedicular width (Figure 3.9) on the chest phantom using the same scan parameters resulted in lower reliability. The interobserver agreement was almost perfect when assessing the pedicle screw placement on the cadaveric pig spine for the scans obtained at 120 kV/128 mAs and 80 kV/80 mAs, and substantial for images at 80 kV/40 mAs. A limitation of using the pig spine might be that there is less scattering material than in a patient. Since it is mainly the impact of artefacts induced by metal implants that degrade the reliability to assess the screw position and not the level of image noise, it is assumed that the pig spine fulfils its purpose.

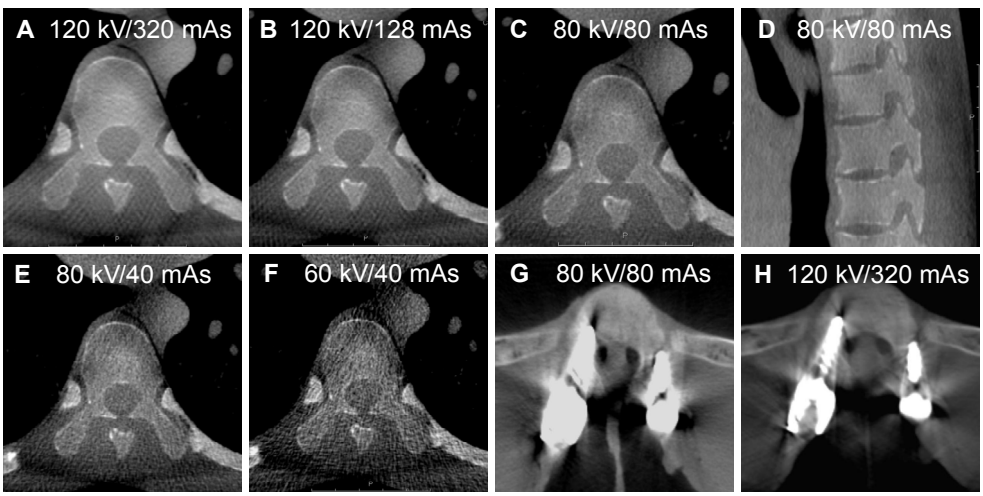

Figure 4.4 Images obtained using the chest phantom and O-arm system at exactly the same vertebral level with different exposure parameters as indicated in each image (A to F). Images show that the delineation of pedicular cortical borders was relatively sharp, even in images E and F. Images obtained by the O-arm system of the cadaveric pig spine operated on with pedicle screws (G to H). Note that both images show that the right screw was normally placed, whereas the left screw was placed lateral to the pedicle.

The effective doses of the O-arm system can be reduced 5 times without a negative impact on image quality with regard to information required for spinal surgery instead of using the scan parameters recommended by the manufacturer (comparing 80 kV/80 mAs and 120 kV/128 mAs). The scan settings recommended by the manufacturer are specified for intra-operative imaging of the chest and abdominal regions in a small patient. This substantial dose reduction is remarkable since the O-arm system is optimised for use in spine, orthopaedic, and trauma-related surgeries. In adult patients with body weight exceeding the average weight at the patient's age, scan settings of 80 kV/128 mAs and 120 kV/128 mAs need to be considered.

4.4 Initial tests of the MADEIRA phantom

Initial measurements from the MADEIRA phantom were presented in **Paper IV**. The phantom was easy to fill using a syringe with a long needle and air bubbles were easily avoided. Figure 4.5 shows SPECT images of the MADEIRA phantom and the evaluation of PVE in the five cones with the highest activity concentration relative to the background activity concentration. The onset of PVE was at a cone diameter of roughly 10 mm. As shown in Figures 4 and 5 in **Paper IV**, the level of reconstructed activity concentration before the onset of PVE was not affected by the number of projections used for reconstruction, but by the diameter of the cone where PVE first occurs. Consequently, a reduction in the number of projections will increase the importance of PVE.

The MADEIRA phantom can also be used to evaluate spatial resolution and detectability with the possibility of simultaneously providing different targets for background activity ratios with linearly changing diameters of active or inactive lesions.

Evaluation of PVE for the PET images found no plateau before the starting point of the PVE (Figure 7 in **Paper IV**). This finding was not expected and indicates that the cones should be constructed with larger base diameters. This finding also shows the importance of the reconstruction process and may be due to the chosen suppression and regularisation mechanism included in the reconstruction algorithms. Unfortunately, it was not possible to change any reconstruction settings in the PET reconstruction algorithm to further investigate its influence of PVE.

To make measurements with the MADEIRA phantom under realistic clinical conditions, the outer vessel was designed to fit into the RSD Alderson heart/thorax phantom (Figure 4.6 A) as an alternative to its lung inserts. A special base-plate has been constructed for the Alderson phantom, and measurements can now be made with the MADEIRA phantom in the thorax phantom.

The figure of merit was to perform one acquisition using the MADERA phantom with very good statistics (large matrix size, large number of projections). The total number of photons can then be varied by simulations (increasing Poisson noise), and images can be reconstructed with a variable number of projections and matrix sizes. In this way, a complete characterisation of a system can be achieved with only one acquisition.

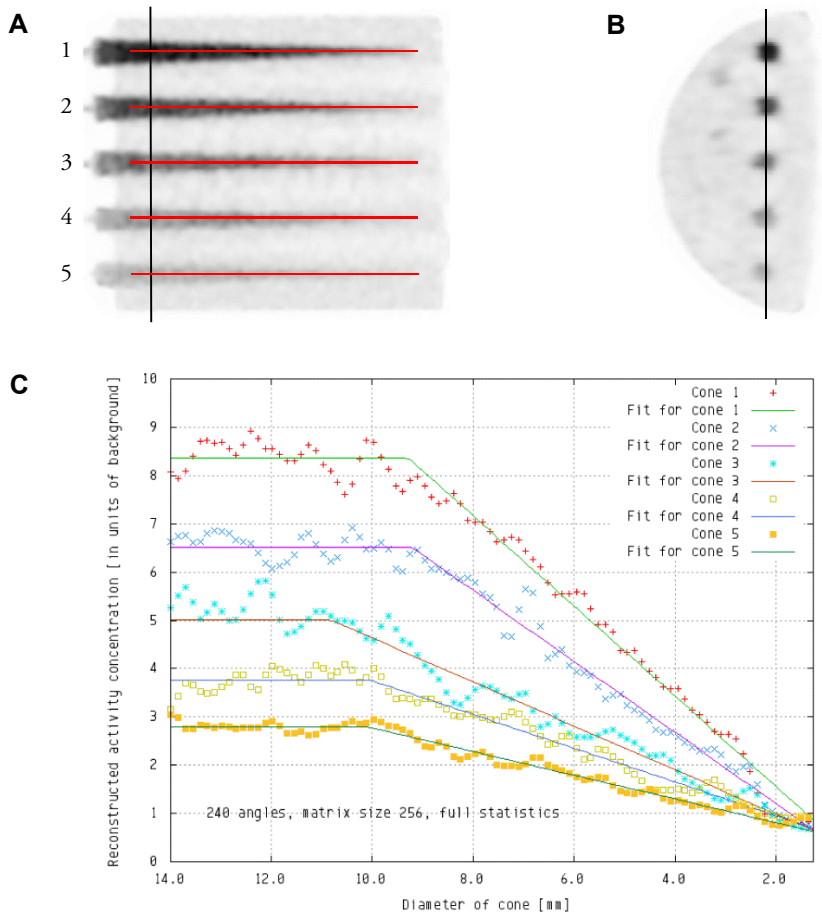

Figure 4.5 Reconstructed coronal (A) and axial (B) SPECT images of the MADEIRA phantom using the iterative algorithm ReSPECT and showing the five cones with the highest activity concentration relative to the background activity concentration. Profiles were drawn in the centre along the length of the cones (indicated as red lines) (A). Reconstructed activity concentration normalised to the background activity concentration (measured in a cone-free area inside the vessel) as a function of the diameter of the cone (C). The onset of PVE occurs at a cone diameter of roughly 10 mm. The axial SPECT image (B) shows the ability of using the MADEIRA phantom for evaluation of visibility of cones with different activity concentration relative to the background activity concentration.

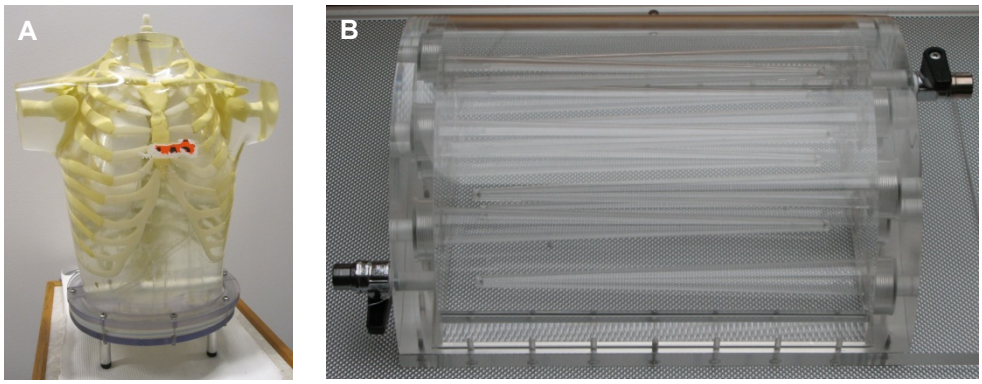

Figure 4.6 A special base-plate has been constructed, which makes it possible to insert the MADEIRA phantom into the RSD Alderson heart/thorax phantom (A). The new version of the MADEIRA phantom contains 12 cones and has two emptying valves (B). Courtesy of U Engeland (Scivis GmbH, Göttingen, Germany).

The cone walls were fabricated to be as thin as possible (1 mm) to minimise the 'wall effect' caused by the shell of zero activity separating the cone solution and background solution. The effect is thought to be negligible in regards to the evaluation of PVE. The 'spill-in' and 'spill-out' effects from other volumes in the cone and from other cones, as well as from the background activity, may be further studied by Monte Carlo simulation.

The MADEIRA phantom has the potential to be a useful and important practical tool for comparing and optimising different acquisition and reconstruction parameters in nuclear medicine tomographic studies. In addition, this new phantom can be used to find the best working point of a given system, as well as for comparisons between various tomographic units. The MADEIRA phantom is now commercially available and the number of cones has been reduced to 12 (Figure 4.6 B). To improve the ease of cleaning, the new version has two emptying valves.

4.5 Evaluation of reconstruction methods for ^{123}I-MIBG-SPECT

SPECT is afflicted with relatively poor spatial resolution and high statistical noise compared to other medical imaging systems. This limitation is partly explained by the restricted amount of reasonable activity, photon attenuation within the patient, scatter, reasonable acquisition time, light scatter in the detector, detector-photomultiplier tube configuration, and the trade-off between efficiency and the

spatial resolution of the collimator. By choosing an appropriate reconstruction method and optimal reconstruction parameters, opportunities exist for improving image quality and lesion detectability. To find the optimal conditions for a reconstruction algorithm, several parameters need to be optimised. The optimal settings depend on, e.g., the clinical task, the target organs, the patient, and the preferences of the observer.

In **Paper V**, ^{123}I-MIBG-SPECT images were visually assessed based on a rank-order method (section 3.3.2). The patients were intravenously injected with approximately 200 MBq, which results in an effective dose of 2.6 mSv (ICRP, 1998). The optimal EI number for Flash 3D was determined to be 32 for both acquisitions (4 h and 24 h p.i.), which is lower than our department default setting of 80. The average rank order (best first) for the different reconstructions for acquisitions 4 h p.i. was Flash $3D_{32}$ > ReSPECT > Flash $3D_{64}$ > OPED, and for acquisitions 24 h p.i. Flash $3D_{16}$ > ReSPECT > Flash $3D_{32}$ > OPED. Examples of the reconstructions are shown in Figure 4.7.

Observer variability concerning optimal EI number and reconstruction algorithm may be explained by differences in individual preferences of what is appropriate image quality. There was disagreement regarding preferable EI for acquisitions 24 h p.i. between the first and second visual assessment, but the results indicate that we should decrease the number of EI. In our department, the number of EI has been reduced from 80 to 32 for acquisitions 4 h and 24 h after injection. However, using too few EI is undesirable as the algorithm may not reach convergence everywhere in the reconstructed volume and lesions will not be visible.

The ReSPECT and OPED algorithms have potential for improvement; CT-based attenuation correction was not implemented as in Flash 3D. In addition, no scatter correction was applied in the OPED algorithm. ReSPECT was evaluated in a previous study of parathyroid scanning with ^{99m}Tc-MIBI (Van Hoorn, 2010). The study demonstrated better image quality using ReSPECT compared to the algorithm HOSEM (Hermes Medical Solutions, Stockholm, Sweden). The reconstructed images using OPED were noisy and had streak-like artefacts due to the geometry of the SPECT data, and no attenuation or scatter correction was applied (Figure 4.7 D). Due to the collimation in SPECT, the measured data are parallel in the classical sense, i.e. uniformly distributed projections with equi-spaced lateral sampling. OPED requires sinusoidal lateral sampling and, consequently, the SPECT data needs to be re-sampled. In general, OPED is more suitable for use in PET and CT (Xu, 2006).

Based on experience from the visual assessment, the Scientific Visualizer software will be further improved and implemented with settings such as linking the window level and slice orientation between the different image sets. The viewer has potential as a very useful tool in the framework of optimising nuclear medicine imaging.

The results obtained in studies like this are specific for the scanner and parameter settings, and the outcome might vary by the amount of radionuclide activity used,

acquisition parameters, acquisition time, and examined body area. Another possible limitation is that the observers might have recognized and were familiar with the Flash 3D reconstructions. The primary selection of a preferred EI number for Flash 3D in the first visual assessment could also have formed a bias in its favour. To reduce this source of bias, the second assessment was carried out a couple of weeks after the first assessment.

Fewer optimisation trials in the form of observer performance studies have been performed for SPECT and PET than for X-ray imaging, and more investigations should be performed to determine the optimal reconstruction conditions and optimal reconstruction method. The conditions and method should be optimised in each department for each type of scanner and clinical task as the type of detector, crystal size, correction methods, etc., differs among the various scanners. This study shows an example of how an optimisation of this kind can be performed. The result of this rank-order study gives an indication of preferred reconstruction parameters and algorithms, which need to be further investigated with a larger patient cohort. The impact on diagnostic performance was not investigated, and there are variations in patient size, shape, and uptake affinity for the radiopharmaceutical that may influence the result. However, the results are useful for future optimisation of reconstruction methods and parameter settings.

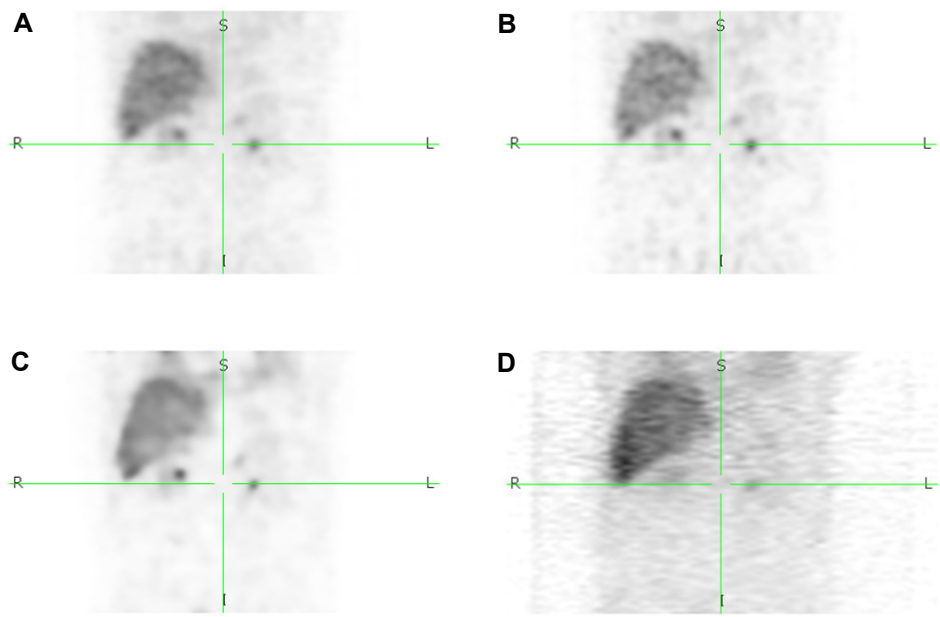

Figure 4.7 Coronal images acquired 4h after the injection of approximately 200 MBq ^{123}I-MIBG and reconstructed using different reconstruction methods: Flash $3D_{32}$ (A), Flash $3D_{64}$ (B), ReSPECT (C), and OPED (D).

5. Conclusions

Clinical application of CT has revolutionised medical imaging and plays a crucial role in routine medical care. Despite a significant reduction of CT doses in recent years, mainly due to improved technology, CT is still a predominant source of medical radiation absorbed dose to the general population. With SPECT/CT and PET/CT, additional information is provided about physiology and cellular and molecular events. However, significant dose contributions are made by SPECT and PET, making PET/CT and SPECT/CT high-dose investigations that need to be assessed from a complete diagnostic chain perspective.

Today, several approaches are used to minimise radiation absorbed dose and improve image quality in medical X-ray and nuclear medicine imaging. One way to succeed is to use an AEC system, which has been shown to be an effective tool for reducing absorbed dose to patients undergoing CT examinations. The reduction ranged from 35-60% for an anthropomorphic chest phantom, depending on the system and AEC settings. The variation in image noise among images obtained along the scanning direction was lower when using the AEC systems, but the image noise generally increased. User-specified variance of the adaptation strengths in the Siemens AEC system can modify image quality or absorbed dose to the patient.

Evaluation of the abdominal CT protocol demonstrated that an increased amount of i.v. CM can compensate for a reduced radiation absorbed dose and vice versa, maintaining the SNR in the liver and CNR for a hypothetical hypovascular liver metastasis. Subjective image quality was affected by an increased noise level in the images, but was judged to be acceptable in all investigated patient groups except the one with the lowest radiation absorbed dose. Using this protocol, the effective dose was reduced by 57% in the youngest patient group and the amount of i.v. CM was reduced by 18% in the elderly group.

Organ doses and effective dose to the patient for the cone-beam O-arm system when used in spinal surgery were estimated by Monte Carlo simulation. The effective dose can be reduced to 1.5-2.4 mSv, which is 5 times lower than using the scan settings recommended by the manufacturer for intra-operative imaging of the chest and abdominal regions in a small patient. Such a dose reduction does not negatively impact image quality with regard to the information required for spinal surgery.

The visual assessment study of ^{123}I-MIBG-SPECT demonstrated that Flash $3D_{32}$ (4 h p.i.) and Flash $3D_{16}$ (24 h p.i.), followed by ReSPECT, were the preferable reconstruction algorithms. An additional technical analysis regarding spatial resolution, PVE, and detectability of the examined reconstruction methods may be performed using the MADEIRA phantom. The MADEIRA phantom has shown potential as a useful and important practical tool in the evaluation and optimisation of nuclear medicine tomography.

5.1 Future aspects

One important matter in diagnostic radiology is that all examinations shall be justified to avoid unnecessary irradiation of the patients. To prevent unjustified examinations a close cooperation between clinicians, radiologists and medical physicists are needed. An efficient cooperation between nuclear medicine and radiology departments is necessary to use CT, SPECT/CT and PET/CT investigations most appropriately. Efforts should be made to better inform referring physicians concerning various radiological examinations, criteria for their use and their dose contribution when optimised.

Today, the detectors from all CT manufactures are based on a scintillator-photodiode design. However, extensive research on energy-resolved photon-counting detectors, which have several promising advantages, is ongoing; two advantages are spectral imaging and higher SNR due to the rejection of electronic noise and scattered radiation (Wang et al., 2011b; Yu et al., 2009). The limitation today is the count rate capability. Ongoing research is also evaluating the potential of high atomic number element-based contrast agents, such as gadolinium, hafnium, and gold, with K-edges in the range of the average spectral energies (Nowak et al., 2011). The goal of using CM based on high atomic number is an increased CNR at equal doses, which would allow for dose reduction. Taking inspiration from nuclear medicine, targeted contrast agents are under investigation. Examples of use are targeted gold nanoparticles for visualisation of atherosclerotic plaques and other diagnostic applications (Boote et al., 2010; Cormode et al., 2010; Hyafil et al., 2007). It is now possible to envision molecular imaging using CT. With further advances in computation technology, the conventional FBP reconstruction procedure is expected to be replaced more and more by comprehensive iterative algorithms in daily clinical practice. Nelson et al. (2011) showed that the use of model-based iterative reconstruction applied to ultra-low dose CT of the chest (0.09 mSv) might replace a chest radiograph.

One of the most recent advances in SPECT imaging is the development of ultra-fast SPECT cameras dedicated to cardiac imaging (Garcia et al., 2011). The new design consists of multiple detectors surrounding the patient to detect the photons from a smaller arc. Conventional thallium-activated sodium iodide (NaI(Tl)) scintillation detectors have been replaced in some systems by solid-state detectors, resulting in improved energy, spatial, and contrast resolution and 5-10 fold increased counting sensitivity, with the potential for an acquisition time of 2 min or less for stress myocardial perfusion scan. Iterative reconstruction methods have been used in SPECT for many years, and research continues to further optimise reconstruction methods by incorporating more exact models of the emission and detection process and include compensation for image-degrading effects (Hutton, 2011).

The concept of using PET in combination with CT has been so successful that none of the major medical imaging manufacturers offers standalone PET scanners. The

advantages of PET/MR systems (Von Schulthess and Schlemmer, 2009) that simultaneously acquire PET and MR data are being clinically evaluated. A potential benefit of performing PET in a strong magnetic field is improved spatial resolution, as the positron range can theoretically be reduced (Raylman et al., 1996). However, Delso et al. (2011) found no significant improvement in spatial resolution due to the positron range reduction effect for ^{18}F at 3T. Another advancement in PET is the incorporation of respiratory gating, which minimise the negative effects of respiratory motion on spatial resolution (Kesner and Kuntner, 2010). The use of time-of-flight, i.e. measuring the time interval between the arrivals of the two annihilation photons, is becoming a standard technology for all major PET scanner manufacturers due to current availability of fast scintillators with high stopping power. The use of time-of-flight will further improve image quality due to better trade-offs between contrast recovery and noise (SNR) (Conti, 2011).

There is still considerable room for optimisation and continuous developments of new technologies aim to optimise image quality and radiation absorbed dose to the patient. These technologies will continue to require close collaboration between medical physicists, manufacturers, radiologists, nuclear medicine physicians, technologists, and referring physicians in order to be effectively and optimally used. The challenge is to establish sufficient image quality for a specific diagnostic task with the lowest effective dose to the patient.

Acknowledgements

This project was partially carried out within the Collaborative Project 'MADEIRA' (www.madeiraproject.eu), cofounded by the European Commission through the EURATOM Seventh Framework Programme (grant agreement FP7-212100).

Support was obtained from the Swedish Radiation Safety Authority (SSI P 1579.07) and the Anna and Edwin Berger foundation.

- - - - - - -

I would like to express my sincere gratitude to my supervisors Sören Mattsson, Mikael Gunnarsson, Sigrid Leide-Svegborn, Peter Leander, Helena Uusijärvi-Lizana, and Sven Valind. Your knowledge, support, and guidance have been very valuable to my work. Sören, your experience, good advice, and criticism of manuscripts has been much appreciated. Thank you for always having your door open for discussions. Mikael, thank you for introducing me to the research field. Your positive enthusiasm makes it a pleasure to work with you. Thank you for sharing your knowledge and finding time for valuable discussions. Sigrid, thank you for sharing your knowledge with me, always in an understandable and educational way. Helena, thank you for valuable discussions and constructive criticism of manuscripts. Peter and Sven, thank you for sharing your medical expertise and advice. Peter, I appreciate working with you and your well-structured manner of working. I am looking forward to continued good cooperation with you in future research projects.

I am very grateful to my co-authors on the papers included in this thesis: Kasim Abul-Kasim, Tobias Fält, Jenny Oddstig, Acke Ohlin, Uwe Engeland, Tilmann Prautzsch, and Oleg Tischenko. Thank you for sharing your experience and knowledge with me. It has been a pleasure working with all of you. Kasim, your efficiency and dedication makes it a pleasure to work with you. Tobias, it is a pleasure working with you, I have learned a lot during our discussions and look forward to continued good cooperation. Jenny, thank you for valuable discussions regarding nuclear medicine. Acke, thank you for sharing your experience and surgical expertise. It was instructive and exciting to observe the surgery procedures. Uwe, Tilmann, and Oleg, thank you for all of your support and help regarding the MADEIRA phantom, ReSPECT, and OPED.

I am very grateful to the radiologists and nuclear medicine physicians at the Diagnostic Centre for Imaging and Functional Medicine at Skåne University Hospital Malmö; Lisa Hörberg, Ingela Carlgren, Eufrozina Selariu, Sabine Garpered, and, Ola Thorsson for image interpretation and medical advice.

I would like to thank Gernot Ebel and his colleagues at Scivis GmbH for a pleasant and interesting visit in Göttingen. Thank you for finding time for my questions.

Thank you also to Pontus Timberg and Daniel Förnvik for discussions and good advice regarding human observer studies, Sune Svensson for your efforts in modifying ViewDEX, and Mats Nilsson for sharing your great knowledge in CT physics.

I would like to thank Christopher Rääf, Pontus Timberg, Tony Svahn, David Minarik, Sven Månsson, and Sonny La for a constructive critical review of this thesis.

To all of my colleagues and friends at the Department of Medical Radiation Physics, Lund University, and at the Department of Radiation Physics, Skåne University Hospital, thank you for your good company.

Finally, I would like to thank my family for good advice and always supporting me. Thank you sister Anna Söderberg for being my excellent poster photographer. A special thanks to Sofie Alriksson for all your support, encouragement, and patience.

References

AAPM: American Association of Physicists in Medicine (2008). The measurement, reporting, and management of radiation dose in CT. AAPM Report No 96.

AAPM: American Association of Physicists in Medicine (2010). Comprehensive methodology for evaluation of radiation dose in X-ray computed tomography. AAPM Report No 111.

AAPM: American Association of Physicists in Medicine (2011). Size-specific dose estimates (SSDE) in pediatric and adult body CT examinations. AAPM Report No 204.

Almén A, Richter S, Leitz W (2008). Number of radiological examinations in Sweden. Swedish Radiation Protection Authority Report 2008:03 (In Swedish).

Almén A, Leitz W, Richter S (2009). National survey on justification of CT-examinations in Sweden. Swedish Radiation Protection Authority Report 2009:03.

Bae KT (2010). Intravenous contrast medium administration and scan timing at CT: considerations and approaches. Radiology 256: 32-61.

Båth M, Månsson LG (2007). Visual grading characteristics (VGC) analysis: a non-parametric rank-invariant statistical method for image quality evaluation. Br J Radiol 80: 169-176.

Båth M (2010). Evaluating imaging systems: practical applications. Radiat Prot Dosim 139: 26-36.

Beekman F, Hutton BR (2007). Multi-modality imaging on track. Eur J Nucl Med Mol Imaging 34: 1410-1414.

Beekman FJ, Slijpen ET, Niessen WJ (1998). Selection of task-dependent diffusion filters for the post-processing of SPECT images. Phys Med Biol 43: 1713-1730.

BEIR: Committee on the Biological Effects of Ionising Radiation (2006). Health risks from exposure to low levels of ionizing radiation. BEIR VII. National Academic Press.

Bongartz G, Golding SJ, Jurik AG, Leonardi E, van Persijn van Meerten E, et al. (1999). European guidelines on quality criteria for computed tomography. Ed. Menzel et al. European Commission. Report EUR 16262.

Bongartz G, Golding SJ, Jurik AG, Leonardi E, van Persijn van Meerten E, et al. (2004). European guidelines for multislice computed tomography. The 2004 CT quality criteria. Appendix A: MSCT dosimetry.

Boone JM (2007). The trouble with $CTDI_{100}$. Med Phys 34: 1364-1371.

Boote E, Fent G, Kattumuri V, Casteel S, Katti K, et al. (2010). Gold nanoparticle contrast in a phantom and juvenile swine: models for molecular imaging of human organs using X-ray computed tomography. Acad Radiol 17: 410-417.

Brambilla M, Cannillo B, Dominietto M, Leva L, Secco C, Inglese E (2005). Characterization of ordered-subsets expectation maximization with 3D post-reconstruction Gauss filtering and comparison with filtered backprojection in ^{99m}Tc SPECT. Ann Nucl Med 19: 75-82.

Brenner DJ, Doll R, Goodhead DT, Hall EJ, Land CE, et al. (2003). Cancer risks attributable to low doses of ionizing radiation: assessing what we really know. Proc Natl Acad Sci 100: 13761-13766.

Brenner DJ, Hall EJ (2007). Computed tomography – an increasing source of radiation exposure. N Engl J Med 357: 2277-2784.

Brownell GL, Burnham CA, Hoop B, Bohning DE (1971). Quantitative dynamic studies using short-lived radioisotopes and positron detection. Proc of the symposium on dynamic studies with radioisotopes in medicine, Rotterdam. August 31 – September 4, 1970. IAEA: 161-172.

Bruce RJ, Djamali A, Shinki K, Michel SJ, Fine JP, et al. (2009). Background fluctuation of kidney function versus contrast-induced nephrotoxicity. Am J Roentgenol 192: 711-718.

Bruyant PP (2002). Analytic and iterative reconstruction algorithms in SPECT. J Nucl Med 43: 1343-1358.

Carlander A, Hansson J, Söderberg J, Steneryd K, Båth M (2008). Clinical evaluation of a dual-side readout technique computed radiography system in chest radiography of premature neonates. Acta Radiol 49: 468-474.

Cherry SR, Sorenson JA, Phelps ME (2003). Physics in nuclear medicine. Third edn. Elsevier.

Christner JA, Zavaletta V, Eusemann C, Walz-Flannigan AI, McCollough CH (2010). Dose reduction in helical CT: dynamically adjustable z-axis x-ray beam collimation. Am J Roentgenol 194: 49-55.

Conti M (2011). Focus on time-of-flight PET: the benefits of improved time resolution. Eur J Nucl Med Mol Imaging 38: 1147-1157.

Cormode DP, Roessl E, Thran A, Skajaa T, Gordon RE, et al. (2010). Atherosclerotic plaque composition: analysis with multicolor CT and targeted gold nanoparticles. Radiology 256: 774-782.

Cristy M, Eckerman KF (1987). Specific absorbed fractions of energy at varoius ages from internal photon sources. I. Methods. Oak Ridge National Laboratory, Oak Ridge, USA.

Dalal T, Kalra MK, Rizzo SM, Schmidt B, Suess C, et al. (2005). Metallic prosthesis: technique to avoid increase in CT radiation dose with automatic tube current modulation in a phantom and patients. Radiology 236: 671-675.

Damadian R (1971). Tumor detection by nuclear magnetic resonance. Science 171: 1151-1153.

Deak PD, Smal Y, Kalender WA (2010). Multisection CT protocols: sex- and age-specific conversion factors used to determine effective dose from dose-length product. Radiology 257: 158-166.

Delso G, Fürst S, Jakoby B, Ladebeck R, Ganter C, et al. (2011). Performance measurements of the Siemens mMR integrated whole-body PET/MR scanner. J Nucl Med 52: 1914-1922.

Dixon RL, Boone JM (2010). Cone beam CT dosimetry: a unified and self-consistent approach including all scan modalities – with or without phantom motion. Med Phys 37: 2703-2718.

Dobbins JT (2000). Image quality metrics for digital systems. In: Handbook of medical imaging. Vol I. Physics and Psychophysics. Ed. Beutel J et al. SPIE Press: 161-222.

Eckelman WC, Reba RC, Kelloff GJ (2008). Targeted imaging: an important biomarker for understanding disease progression in the era of personalized medicine. Drug Discov Today 13: 748-759.

European Commission (2001). Radiation protection 118. Referral guidelines for imaging. Office for Official Publication of the European Communities, Luxemburg.

Fleischmann D, Boas FE (2011). Computed tomography – old ideas and new technology. Eur Radiol 21: 510-517.

Flohr T, Ohnesorge BM (2007). Multi-slice CT technology. In: Multi-slice and dual-source CT in cardiac imaging: Principles – Protocols – Indications – Outlook. Second edn. Ed. Ohnesorge BM et al. Springer: 41-69.

Frush DP (2008). Pediatric dose reduction in computed tomography. Health Phys 95: 518-527.

Funama Y, Awai K, Nakayama Y, Kakel K, Nagasue N, et al. (2005). Radiation dose reduction without degradation of low-contrast detectability at abdominal multisection CT with a low-tube voltage technique: phantom study. Radiology 237: 905-910.

F.X. Massé Associates Inc. Health and Medical Physics Consultants (2009). Medtronic Navigation dosimetry report for the Medtronic O-arm system. Medtronic Navigation Inc, Littleton, USA.

Garcia EV, Faber TL, Esteves FP (2011). Cardiac dedicated ultrafast SPECT cameras: new designs and clinical implications. J Nucl Med 52: 210-217.

Good WF, Sumkin JH, Dash N, Johns CM, Zuley ML, et al. (1999). Observer sensitivity to small differences: a multipoint rank-order experiment. Am J Roentgenol 173: 275-278.

Groch MW, Erwin WD (2000). SPECT in the year 2000: basic principles. J Nucl Med Technol 28: 233-244.

Gupta R, Cheung AC, Bartling SH, Lisauskas J, Grasruck M, et al. (2008). Flat-panel volume CT: fundamental principles, technology, and applications. Radiographics 28: 2009-2022.

Gutierrez D, Schmidt S, Denys A, Schnyder P, Bochud FO, Verdun FR (2007). CT-automatic exposure control devices: what are their performances? Nuclear Instruments and Methods in Physcis Research. Section A: Accelerators, Spectrometers, Detectors and Associated Equipment 580: 990-995.

Hadid L, Desbrée A, Schlattl H, Franck D, Blanchardon E, Zankl M (2010). Application of the ICRP/ICRU reference computational phantoms to internal dosimetry: calculation of specific absorbed fractions of energy for photons and electrons. Phys Med Biol 55: 3631-3641.

Håkansson M, Svensson S, Zachrisson S, Svalkvist A, Båth M, Månsson LG (2010). ViewDEX: an efficient and easy-to-use software for observer performance studies. Radiat Prot Dosim 139: 42-51.

Hawman E, Vija AH, Daffach R, Ray M (2003). Flash 3D technolgy optimizing SPECT quality and accuracy. Whitepaper. Siemens Medical Solutions, Forchheim, Germany: 1-6.

He W, Huda W, Magill D, Tavrides E, Yao H (2010). Patient doses and projection angel in cone beam CT. Medical Physics 37: 2359-2368.

Heiken JP, Menias CO, Elsayes K (2006). Liver. In: Computed body tomography with MRI correlation. Fouth edn. Vol 1. Ed. Lee J, et al. Lippincott Williams & Wilkins: 829-930.

Hicks RJ, Lau EWF, Binns DS (2007). Hybrid imaging is the future of molecular imaging. Biomed Imaging Interv J 3: e49.

Hoeschen C, Mattsson S, Cantone MC, Mikuz M, Lacasta C, et al. (2010). Minimising activity and dose with enhanced image quality by radiopharmaceutical administrations. Radiat Prot Dosim 139: 69-74.

Hoffman EJ, Huang SC, Phelps ME (1979). Quantitation in positron emission computed tomography: 1. Effect of object size. J Comput Assist Tomogr 3: 299-308.

Hounsfield GN (1976). Historical notes on computerized axial tomography. J Can Assoc Radiol 27: 135-142.

Houten JK, Nasser R, Baxi N (2011). Clinical assessment of percutaneous lumbar pedicle screw placement using the O-arm multidimensional surgical imaging system. Neurosurgery: Epub ahead of print.

Hsieh J (2009). Computed tomography: principles, designs, artifacts, and recent advances. Second edn. Ed. Hsieh J. SPIE and John Wiley & Sons: 55-117, 375-465.

Hu H (1999). Multi-slice helical CT: scan and reconstruction. Med Phys 26: 5-18.

Huda W, Ogden KM, Khorasani MR (2008). Converting dose-length product to effective dose at CT. Radiology 248: 995-1003.

Hudson HM, Larkin RS (1994). Accelerated image reconstruction using ordered subsets of projection data. IEE Trans Med Imaging 13: 601-609.

Hutton BF, Hudson HM, Beekman FJ (1997). A clinical perspective of accelerated statistical reconstruction. Eur J Nucl Med 24: 797-808.

Hutton BF, Nuyts J, Zaidi H (2006). Iterative reconstruction methods. In: Quantitative analysis in nuclear medicine. Ed. Zaidi H. Springer: 107-140.

Hutton BF (2011). Recent advances in iterative reconstruction for clinical SPECT/PET and CT. Acta Oncol 50: 851-858.

Hyafil F, Cornily JC, Feig JE, Gordon R, Vucic E, et al. (2007). Noninvasive detection of macrophages using a nanoparticulate contrast agent for computed tomography. Nat Med 13: 636-641.

IAEA: International Atomic Energy Agency (2007). Dosimetry in diagnostic radiology: an international code of practise. Technical reports series no. 457.

ICRP: International Commission on Radiological Protection (1988). Radiation dose to patients from radiopharmaceuticals. ICRP Publication 53. Ann. ICRP 18(1-4).

ICRP: International Commission on Radiological Protection (1991). Recommendations of the International Commission on Radiological Protection. Publication 60. Ann. ICRP 21(1-3).

ICRP: International Commission on Radiological Protection (1998). Radiation dose to patients from radiopharmaceuticals. Addendum to ICRP Publication 53. ICRP Publication 80. Ann. ICRP 28(3)

ICRP: International Commission on Radiological Protection (2000). Managing patient dose in computed tomography. ICRP Publication 87. Ann. ICRP 30(4).

ICRP: International Commission on Radiological Protection (2007a). Managing patient dose in multi-detector computed tomography (MDCT). ICRP Publication 102. Ann. ICRP 37(1).

ICRP: International Commission on Radiological Protection (2007b). The 2007 recommendations of the International Commission on Radiological Protection. ICRP Publication 103. Ann. ICRP 37(2-4).

ICRP: International Commission on Radiological Protection (2008). Radiation dose to patients from radiopharmaceuticals. Addendum 3 to ICRP Publication 53. ICRP 106. Ann. ICRP 38(1-2).

ICRP: International Commission on Radiological Protection (2009). Adult reference computational phantoms. ICRP Publication 110. Ann. ICRP 39(2).

ICRU: International Commission on Radiation Units and Measurements (1996). Medical imaging – the assessment of image quality. ICRU report 54.

ICRU: International Commission on Radiation Units and Measurements (1998). Fundamental quantities and units for ionizing radiation. ICRU report 60.

ICRU: International Commission on Radiation Units and Measurements (2008). Receiver operating characteristic analysis in medical imaging. ICRU report 79.

IEC: International Electrotechnical Commission (2009). Medical electrical equipment. Part 2-44: Particular requirements for the basic safety and essential performance of X-ray equipment for computed tomography. IEC 60601-2-44. Third edn.

Johnson TRC, Kalender WA (2011). Physical background. In: Dual energy CT in clinical practice Part I Physical implementation. Ed. Johnson TRC et al. Springer: 3-9.

Jones DP, Robertson PA, Lunt B, Jackson S (2000). Radiation exposure during fluoroscopically assisted pedicle screw insertion in the lumbar spine. Spine 25: 1538-1541.

Kalender WA (2005). Principles of computed tomography. In: Computed tomography: fundamentals, system technology, image quality, applications. Second edn. Ed. Kalender WA. Publics Corporate Publishing: 17-35.

Kalender WA, Buchenau S, Deak P, Kellermeier M, Langner O, et al. (2008). Technical approaches to the optimisation of CT. Phys Med 24: 71-79.

Kalender WA, Deak P, Kellermeier M, van Straten M, Vollmar SV (2009). Application- and patient size-dependent optimization of x-ray spectra for CT. Med Phys 36: 993-1007.

Kalra M K, Maher MM, Toth TL, Hamberg LM, Blake MA, et al. (2004). Strategies for CT radiation dose optimization. Radiology 230: 619-628.

Kalra MK, Maher MM, Toth TL, Schmidt B, Westerman BL, et al. (2005). Reducing radiation dose in emergency computed tomography with automatic exposure control techniques. Emerg Radiol 11: 267-274.

Kalra MK, Brady TJ (2006). CARE Dose 4D new technique for radiation dose reduction. Siemens SOMATOM Sessions 19: 28-31.

Kanematsu M, Kondo H, Goshima S, Kato H, Tsuge U, et al. (2006). Imaging liver metastaes: review and update. Eur J Radiol 58: 217-228.

Katzberg RW, Barrett BJ (2007). Risk of iodinated contrast material – induced nephropathy with intravenous administration. Radiology 243: 622-628.

Katzberg RW, Newhouse JH (2010). Intravenous contrast medium-induced nephrotoxicity: is the medical risk really as great as we have come to believe? Radiology 256: 21-28.

Keat N (2005). CT scanner automatic exposure control systems. Medicines and Healthcare products Regulatory Agency (MHRA) evaluation report 05016.

Keat N (2011). ImPACT CT patient dosimetry calculator (version 1.0.4). ImPACT (www.impactscan.org/ctdosimetry.htm).

Kesner AL, Kuntner C (2010). A new fast and fully automated software based algorithm for extracting respiratory signal from raw PET data and its comparison to other methods. Med Phys 37: 5550-5559.

Kondo H, Kanematsu M, Goshima S, Tomita Y, Kim MJ, et al. (2010). Body size indexes for optimizing iodine dose for aortic and hepatic enhancement at multidetector CT: comparsion of total body weight, lean body weight, and blood volume. Radiology 254: 163-169.

Korn A, Fenchel M, Bender B, Danz S, Hauser TK, et al. (2011). Iterative reconstruction in head CT: image quality of routine and low-dose protocols in comparison with standard filtered back-projection. Am J Neuroradiol: Epub ahead of print.

Kuhl DE, Edwards RQ (1963). Image separation radioisotope scanning. Radiology 80: 653-662.

Lange K, Carson R (1984). EM reconstruction algorithms for emission and transmission tomography. J Comput Assist Tomogr 8: 306-316.

Leander P, Söderberg M, Fält T, Gunnarsson M, Albertsson I (2010). Post-processing image filtration enabling dose reduction in standard abdominal CT. Radiat Prot Dosim 139: 180-185.

Ledenius K, Stålhammar F, Wiklund LM, Fredriksson C, Forsberg A, Thilander-Klang A (2010). Evaluation of image-enhanced paediatric computed tomography brain examinations. Radiat Prot Dosim 139: 287-292.

Leitz W, Axelsson B, Szendrö G (1995). Computed tomography dose assessment – a pratical approach. Radiat Prot Dosim 57: 377-380.

Lewellen T, Karp J (2004). PET systems. In: Emission tomography – the fundamentals of PET and SPECT. Ed. Wernick MN, Aarsvold JN. Elsevier Academic Press: 179-194.

Liow JS, Strother SC (1993). The convergence of object dependent resolution in maximum likelihood based tomographic image reconstruction. Phys Med Biol 38: 55-70.

Månsson LG (2000). Methods for the evaluation of image quality: a review. Radiat Prot Dosim 90: 89-99.

Mattsson S, Båth M, Hoeschen C, Tingberg A (2010). Medical imaging-optimisation in X-ray and molecular imaging. Radiat Prot Dosim 139: 1-2.

Mattsson S, Söderberg M (2011a). Radiation dose management in CT, SPECT/CT and PET/CT techniques. Radiat Prot Dosim 147: 13-21.

Mattsson S, Johansson L, Leide-Svegborn S, Liniecki J, Nosske D, Riklund K, Stabin M, Taylor D (2011b). Current activities in the ICRP concerning estimation of radiation doses to patients from radiopharmaceuticals for diagnostic use. J Phys Conf Ser 317: 1-6.

Mayo JR, Leipsic JA (2009). Radiation dose in cardiac CT. Am J Roentgenol 192: 646-653.

McCollough CH, Bruesewitz MR, Kofler J M (2006). CT dose reduction and dose management tools: overview of available options. Radiographics 26: 503-512.

McCullough PA, Adam A, Becker CR, Davidson C, Lameire N, et al. (2006). Risk prediction of contrast-induced nephropathy. Am J Cardiol 18: 27K-36K.

Medtronic (2009). Clinical value of the O-arm imaging system & Stealth Station navigation: overview of journal publications. Medtronic Navigation Inc, Littleton, USA: 1-15.

Medtronic (2010). O-arm imaging system user manual: specifications. BI-500-00095. Revision 2. Medtronic Navigation Inc, Littleton, USA: 10.4-10.6.

Morcos SK, Thomsen HS, Webb JA (1999). Contrast-media-induced nephrotoxicity: a consensus report. Contrast Media Safety Committee, European Society of Urogenital Radiology (ESUR). Eur Radiol 9: 1602-1613-

Mulkens TH, Bellinck P, Baeyaert M, Ghysen D, Van Dijck X, et al. (2005). Use of an automatic exposure control mechanism for dose optimization in multi-detector row CT examinations: clinical evaluation. Radiology 237: 213-223.

Nagel HD, Stumpp P, Kahn T, Gosh D (2011). Performance of an automatic dose control system for CT: specifications and basic phantom tests. Rofo 183: 60-67.

Namasivayam S, Kalra MK, Torres WE, Small WC (2006). Adverse reactions to intravenous iodinated contrast media: a primer for radiologists. Emerg Radiol 12: 210-215.

NCRP: National Council on Radiation Protection and Measurements (2009). Ionizing radiation exposure of the population of the United States. NCRP Report No. 160.

Nelson RC, Feuerlein S, Boll DT (2011). New iterative reconstruction techniques for cardiovascular computed tomography: how do they work, and what are the advantages and disadvantaged? J Cardiovasc Comput Tomogr 5: 286-292.

Nottmeier EW, Seemer W, Young PM (2009). Placement of thoracolumbar pedicle screws using three-dimensional image guidance: experience in a large patient cohort. J Neurosurg Spine 10: 33-39.

Nowak T, Hupfer M, Brauweiler R, Eisa F, Kalender WA (2011). Potential of high-Z contrast agents in clinical contrast enhanced computed tomography. Med Phys 38: 6469-6482.

Oikarinen H, Meriläinen S, Pääkkö E, Karttunen A, Nieminen MT, Tervonen O (2009). Unjustified CT examinations in young patients. Eur Radiol 19: 1161-1165.

Papadakis AE, Perisinakis K, Damilakis J (2008). Automatic exposure control in pediatric and adult multidetector CT examinations: a phantom study on dose reduction and image quality. Med Phys 35: 4567-4576.

Papadakis AE, Perisinakis K, Oikonomou I, Damilakis J (2011). Automatic exposure control in pediatric and adult computed tomography examinations: can we estimate organ and effective dose from mean mAs reduction? Invest Radiol 46: 654-662.

Prakash P, Kalra MK, Kambadakone AK, Pien H, Hsieh J, et al. (2010). Reducing abdominal CT radiation dose with adaptive statistical iterative reconstruction technique. Invest Radiol 45: 202-210.

Preston DL, Shimizu Y, Pierce DA, Suyama A, Mabuchi K (2003). Studies of mortality of atomic bomb survivors. Report 13: Solid cancer and noncancer disease mortality: 1950-1997. Radiat Res 160: 381-407.

Ratib O, Beyer T (2011). Whole-body hybrid PET/MRI: ready for clinical use? Eur J Nucl Med Mol Imaging 38: 992-995.

Raylman RR, Hammer BE, Christensen NL (1996). Combined MRI-PET scanner: a Monte Carlo evaluation of the improvements in PET resolution due to the effects of a static homogeneous magnetic field. IEE Trans Nucl Sci 43: 2406-2412.

Rizzo S, Kalra M, Schmidt M, Dalal T, Suess C, et al. (2006). Comparison of angular and combined automatic tube current modulation techniques with constant tube current CT of the abdomen and pelvis. Am J Roentgenol 186: 673-679.

Rousset OG, Zaidi H (2006). Correction for partial volume effects in emission tomography. In: Quantitative analysis in nuclear medicine imaging. Ed. Zaidi H. Springer: 236-271.

Rundback JH, Nahl D, Yoo V (2011). Contrast-induced nephropathy. J Vasc Surg 54: 575-579.

Santos ER, Ledonio CG, Castro CA, Truong WH, Sembrano JN (2012). The accuracy of intraoperative O-arm images for the assessment of pedicle screw position. Spine: 37: E119-E125.

Scivis GmbH (2006). ReSPECT – Technical description. Version 2.0. Scivis, Göttingen, Germany: 1-27.

Shepp LA, Vardi Y (1982). Maximum likelihood reconstruction for emission tomography. IEEE Trans Med Imaging 1: 113-122.

Shope TB, Gagne RM, Johnson GC (1981). A method for describing the doses delivered by transmission x-ray computed tomography. Med Phys 8: 488-495.

Shrimpton PC (2004). Assessment of patient dose in CT. Chilton, NRPB-PE/1/2004.

Silverman PM, Kalender WAm Hazle JD (2001). Common terminology for single and multislice helical CT. Am J Roentgenol 176: 1135-1136.

Singh S, Kalra MK, Thrall JH, Mahesh M (2011). Automatic exposure control in CT: applications and limitations. J Am Coll Radiol 8: 446-449.

Skretting A (2009). 'Intensity diffusion' is a better description than 'partial volume effect'. Eur J Nucl Med Mol Imaging 36: 536-537.

Smedby Ö, Fredrikson M (2010). Visual grading regression: analysing data from visual grading experiments with regression models. Br J Radiol 83: 767-775.

Söderberg M, Gunnarsson M, Nilsson M (2010). Simulated dose reduction by adding artificial noise to measured raw data: a validation study. Radiat Prot Dosim 139: 71-77.

Solomon RJ, Mehran R, Natarajan MK, Doucet S, Katholi RE, et al. (2009). Contrast-induced nephropathy and long-term adverse events: cause and effect? Clin J Am Soc Nephrol 4: 1162-1169.

Stabin M (2006). Nuclear medicine dosimetry. Phys Med Biol 51: 187-202.

Stacul F, van der Molen, Reimer P, Webb JA, Thomsen HS, et al. (2011). Contrast induced nephropathy: updated ESUR contrast media safety committee guidelines. Eur Radiol 21: 2527-2541.

Stamm G, Nagel HD (2002). CT-Expo – a novel program for dose evaluation in CT. Fortschr Röntgenstr 174: 1570-1576 (In German).

Sterner G, Hellström M, Lagerqvist B, Aspelin P, Nyman U (2009). X-ray contrast media and renal failure. Better understanding of risk markers and follow up are needed. Läkartidningen 106: 1737-1742 (In Swedish).

Tapiovaara M, Siiskonen T (2008). PCXMC – a Monte Carlo program for calculating patient doses in medical X-ray examinations. STUK-A231. Second edn.

Tischenko O, Xu Y, Hoeshcen C (2010). Main features of the tomographic reconstruction algorithm OPED. Radiat Prot Dosim 139: 204-207.

Toprak O, Cirit M (2006). Risk factors for contras-induced nephropathy. Kidney Blood Press Res 29: 84-93.

Towers JD, Holbert JM, Britton CA, Costello P, Sciulli R, et al. (2000). Multipoint rank-order study methodology: observer issues. Invest Radiol 35: 125-130.

Townsend DW (2008). Multimodality imaging of structure and function. Phys Med Biol 53: R1-R39.

Tsui BMW, Frey EC (2006). Analytic image reconstruction methods in emission computed tomography. In: Quantitative analysis in nuclear medicine. Ed. Zaidi H. Springer: 82-106.

Tzedakis A, Damilakis J, Perisinakis K, Stratakis J (2005). The effect of z overscanning on patient effective dose from multidetector helical computed tomography examinations. Med Phys 32: 1621-1629.

UNSCEAR: United Nations Scientific Committee on the Effects of Atomic Radiation (2008). UNSCEAR 2006 Report Vol I: Effects of ionizing radiation.

UNSCEAR: United Nations Scientific Committee on the Effects of Atomic Radiation (2010). UNSCEAR 2008 Report Vol I: Sources and effects of ionizing radiation.

UNSCEAR: United Nations Scientific Committee on the Effects of Atomic Radiation (2011). UNSCEAR 2010 Report: Summary of low-dose radiation effects on health.

Vallabhajosula S, Nikolopoulou A (2011). Radioiodinated metaiodobenzylguanidine (MIBG): radiochemistry, biology, and pharmacology. Semin Nucl Med 41: 324-333.

Van Hoorn R, Vriens D, Postema J (2010). Evaluation of advanced ReSPECT image reconstruction software in a phantom model and in parathyroid scanning. J Nucl Med 51: 1352 (abstract).

Vandenberghe S, D'Asseler Y, Van de Walle R, Kauppinen T, Koole M, et al. (2001). Iterative reconstruction algorithms in nuclear medicine. Comput Med Imaging Graph 25: 105-111.

Wang J, Duan X, Christner JA, Leng S, Yu L, McCollough CH (2011a). Radiation dose reduction to the breast in thoracic CT: comparison of bismuth shielding, organ-based tube current modulation, and use of a globally decreased tube current. Med Phys 38: 6084-6092.

Wang X, Meier D, Taguchi K, Wagenaar DJ, Patt BE, Frey EC (2011b). Material separation in x-ray CT with energy resolved photon-counting detectors. Med Phys 38: 1534-1546.

Watanabe H, Kanematsu M, Miyoshi T, Goshima S, Kondo H, et al. (2010). Improvement of image quality of low radiation dose abdominal CT by increasing contrast enhancement. Am J Roentgenol 195: 986-992.

Winklehner A, Karlo C, Puippe G, Schmidt B, Flohr T, et al. (2011). Raw data-based iterative reconstruction in body CTA: evaluation of radiation dose saving potential. Eur Radiol 21: 2521-2526.

Vollmar SV, Kalender WA (2008). Reduction of dose to the female breast in thoracic CT: a comparison of standard-protocol, bismuth-shielded, partial and tube-current-modulated CT examinations. Eur Radiol 18: 1674-1682.

Von Schulthess GK, Schlemmer HP (2009). A look ahead: PET/MR versus PET/CT. Eur J Nucl Med Mol Imaging 36 Suppl 1: S3-S9.

Xu Y, Tischenko O, Hoeschen C (2006). A new reconstruction algorithm for radon data. Proc SPIE 6142: 791-798.

Xu Y, Tischenko O, Hoeschen C (2007). Image reconstruction by OPED algorithm with averaging. Numer Algor 45: 179-193.

Yu L, Liu X, Leng S, Kofler JM, Ramirez-Giraldo JC, et al. (2009). Radiation dose reduction in computed tomography: techniques and future perspective. Imaging Med 1: 65-84.

Zeng GL, Galt JR, Wernick MN, Mintzer R, Aarsvold JN (2004). Single-photon emission computed tomography. In: Emission tomography – the fundamentals of PET and SPECT. Ed. Wernick MN, Aarsvold JN. Elsevier Academic Press: 127-152.

Zhang J, Weir V, Fajardo L, Lin J, Hsiung H, Ritenour ER (2009). Dosimetric characterization of a cone-beam O-arm imaging system. J Xray Sci Technol 17: 305-317.